

Rotatable Antenna Enabled Wireless Communication: Modeling and Optimization

Beixiong Zheng, *Senior Member, IEEE*, Qingjie Wu, and Rui Zhang, *Fellow, IEEE*

1

Abstract—**Fluid antenna system (FAS) and movable antenna (MA)** have recently emerged as promising technologies to exploit new degrees of freedom (DoFs) in the spatial domain, which have attracted growing attention in wireless communication. In this paper, we propose a new rotatable antenna (RA) model to improve the performance of wireless communication systems. In this paper, we propose a new rotatable antenna (RA) model to improve the performance of wireless communication systems. Different from conventional fixed antennas, the proposed RA system can flexibly alter the three-dimensional (3D) boresight direction of each antenna independently by adjusting its deflection angles to achieve a desired array directional gain pattern. Specifically, we investigate an RA-enabled uplink communication system, where the receive beamforming and the deflection angles of all RAs at the base station (BS) are jointly optimized to maximize the minimum signal-to-interference-plus-noise ratio (SINR) among all the users. In the special single-user and free-space propagation setup, the optimal deflection angles of RAs are derived in closed form with the maximum-ratio combining (MRC) beamformer applied at the BS. Moreover, we analyze the asymptotic performance with an infinite number of antennas based on this solution, which theoretically proves that the RA system can achieve a higher array gain as compared to the fixed-antenna system. In the general multi-user and multi-path channel setup, we first propose an alternating optimization (AO) algorithm to alternately optimize the receive beamforming and the deflection angles of RAs in an iterative manner. Then, a two-stage algorithm that solves the formulated problem without the need for iteration is further proposed to reduce computational complexity. Simulation results are provided to validate our analytical results and demonstrate that the proposed RA system can significantly outperform other benchmark schemes.

Index Terms—Rotatable antenna (RA), near-field modeling, array directional gain pattern, performance analysis, pointing vector optimization, antenna boresight, antenna orientation.

I. INTRODUCTION

In the rapidly evolving landscape of global information and communications technology (ICT), the forthcoming sixth-generation (6G) wireless network is envisioned to support even more densely-connected users and devices across more diverse applications and services, thus demanding significantly higher performance targets compared to its preceding generations [1]. Undoubtedly, as one of the most critical technologies for the current fifth-generation (5G) mobile communication, multiple-input-multiple-output (MIMO) can dramatically enhance the transmission rate and reliability of wireless networks through beamforming and multiplexing via multiple antennas at the transceivers [2]. However, the channel capacity and spectrum efficiency achieved by conventional MIMO are insufficient to meet the stringent requirements of 6G in its new applications.

(Corresponding authors: Beixiong Zheng and Rui Zhang.)

B. Zheng and Q. Wu are with the School of Microelectronics, South China University of Technology, Guangzhou 511442, China (e-mail: bxzheng@scut.edu.cn; mjqwu@mail.scut.edu.cn).

R. Zhang is with the School of Science and Engineering, Shenzhen Research Institute of Big Data, The Chinese University of Hong Kong, Shenzhen 518172, China (e-mail: rzhang@cuhk.edu.cn). He is also with the Department of Electrical and Computer Engineering, National University of Singapore, Singapore 117583 (e-mail: elezhang@nus.edu.sg).

To further improve the spatial resolution and degree of freedom (DoF), wireless networks tend to integrate drastically more antennas into arrays at the base station (BS), thereby advancing MIMO to massive MIMO, and even further to extremely large-scale MIMO [3]–[6].

Although larger-scale MIMO can offer substantial array and spatial multiplexing gains, it comes at the expense of much higher hardware costs and power consumption. Furthermore, increasing the number of antennas cannot fully exploit the spatial DoFs, since the traditional fixed antennas cannot change their positions or orientations flexibly once deployed. Recently, fluid antenna system (FAS) and movable antenna (MA) have been proposed as promising technologies to overcome this limitation and attracted growing attention in wireless communication [7]–[11]. Compared to fixed-antenna architecture, FAS/MA enables the local movement of antennas in a specified region through different antenna movement mechanisms, which can proactively reshape the wireless channels to more favorable conditions and thus achieve higher capacity without increasing the number of antennas. Furthermore, with such a new DoF offered at the physical layer, it has been validated that FAS/MA can achieve various significant performance advantages, including interference mitigation, flexible beamforming, and multiplexing enhancement [12]–[14]. By leveraging these capabilities of FAS/MA, substantial efforts have been devoted to integrating them with cutting-edge wireless technologies, such as integrated sensing and communications (ISAC) [15], unmanned aerial vehicle (UAV) communications [16], intelligent reflecting surface (IRS) [17]–[19], and over-the-air computation [20]. Nevertheless, while FAS/MA can bring numerous performance advantages, their practical implementation is highly constrained by the response time and/or movement speed of the antennas. Additionally, existing works on FAS/MA still face limitations in terms of spatial flexibility and performance enhancement since only the positions of antennas are adjusted while their orientations are fixed.

To fully exploit all six-dimensional (6D) spatial DoFs, 6D movable antenna (6DMA) has been recently proposed to flexibly adjust both the three-dimensional (3D) position and 3D rotation of distributed antennas/arrays [21]–[23]. Based on the long-term/statistical user channel distribution, the 6DMA-equipped transceiver can adaptively allocate its antenna resources to improve the array and spatial multiplexing gains. Additionally, 6DMA can achieve both array and geometric gains to enhance the performance of wireless sensing [24]. Although 6DMA provides a general model for position and rotation adjustable antennas, its implementation requires drastic changes of the current antenna architectures of existing BSs and thus may be practically cost-prohibitive. In addition, many new practical movement and rotation constraints should be considered in 6DMA systems [21]–[23], making the joint design of positions and rotations of all 6DMA arrays highly

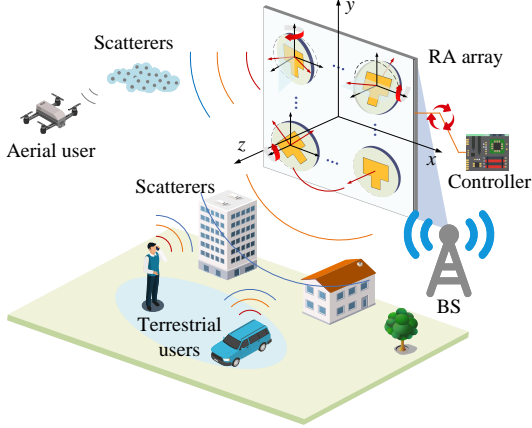


Fig. 1. An RA-enabled uplink communication system.

challenging and sophisticated.

Motivated by the above, we propose in this paper a new antenna architecture, called rotatable antenna (RA), as a simplified implementation of 6DMA to improve the performance of wireless communications cost-effectively. In the RA system, the deflection angles of each directional antenna can be independently adjusted to change its 3D orientation/boresight, while its 3D position is kept constant to reduce the hardware cost and time/energy overhead associated with antenna position changes in 6DMA. Compared to the conventional fixed-antenna architecture, RA can enhance communication and sensing performance substantially by flexibly adjusting the antenna orientation/boresight within the full 3D space. In this way, RA provides a practical solution for enhancing array gains in desired directions to boost the transmit/received signal power, while reducing the radiation power in undesired directions to avoid information leakage and interference. Therefore, by strategically designing the beamforming and antenna orientation/boresight, the RA system can be deployed to further improve the array/multiplexing gain and enhance the sensing resolution/range in various applications, such as ISAC, massive machine-type communication (mMTC), simultaneous localization and mapping (SLAM), and so on.

Given the above technical advantages and potential applications of RA, we aim to investigate in this paper the system modeling, performance analysis, and optimization algorithm design for an RA-enabled uplink communication system as shown in Fig. 1. The main contributions of this paper are summarized as follows:

- Since the adjustment of antenna orientation/boresight should consider both the propagation environment and the antenna directional gain pattern, we first introduce a pair of deflection angles to characterize the 3D boresight for each RA, and then present a new multi-path geometric near-field channel model related to the antenna deflection angles. Under this channel model, a minimum signal-to-interference-plus-noise ratio (SINR) maximization problem is formulated to jointly optimize the receive beamforming and the deflection angles of all RAs.
- For the special single-user and free-space propagation setup with the maximum-ratio combining (MRC) beamformer applied at the BS, the optimal deflection angles

of RAs are derived in closed form. Meanwhile, a closed-form expression and lower/upper bounds for the signal-to-noise ratio (SNR) under the uniform linear/planar array (ULA/UPA) setting are also derived, showing that the resultant SNR first increases linearly with the number of antennas and eventually converges to a certain limit. Additionally, an asymptotic analysis is provided for the case with an infinite number of antennas to theoretically demonstrate that with a larger range for antenna boresight adjustment, the proposed RA-enabled system can exploit more spatial DoFs to achieve a higher array gain.

- For the general multi-user and multi-path channel setup, to tackle the formulated min-SINR maximization problem for balancing the array directional gains among different users over their multi-path channels, we first propose an alternating optimization (AO) algorithm that alternately optimizes the receive beamforming and the deflection angles of RAs in an iterative manner until convergence is attained. In particular, with the optimal minimum mean-square error (MMSE) beamformer applied at the BS, the subproblem that optimizes the deflection angles of RAs is first transformed into a pointing vector optimization problem and then solved by the successive convex approximation (SCA) technique. To reduce computational complexity, we further propose a two-stage algorithm that solves a weighted channel power gain maximization problem based on the zero-forcing (ZF) beamformer without the need for iteration.
- Simulation results validate our theoretical analysis and demonstrate that the proposed RA-enabled system can significantly improve communication performance over various benchmark schemes. It is shown that with only a small range for antenna boresight adjustment, the RA-enabled system can reap considerable performance gains over the fixed-antenna system. Furthermore, the performance advantages of RAs in flexibly balancing the directional gain over multi-path channels become more pronounced with stronger antenna directivity.

The remainder of this paper is organized as follows. Section II introduces the system model and problem formulation for designing the RA-enabled wireless communication system. In Section III, we derive the optimal closed-form solution and analyze the asymptotic performance under the single-user setup. Section IV proposes the AO algorithm and the two-stage algorithm to solve the formulated problem under the multi-user setup. Section V presents simulation results to evaluate the performance of the proposed system and algorithms. Finally, we conclude the paper in Section VI.

Notation: Upper-case and lower-case boldface letters denote matrices and column vectors, respectively. Superscripts $(\cdot)^T$, $(\cdot)^H$, and $(\cdot)^{-1}$ stand for the transpose, Hermitian transpose, and matrix inversion operations, respectively. The sets of $a \times b$ dimensional complex and real matrices are denoted by $\mathbb{C}^{a \times b}$ and $\mathbb{R}^{a \times b}$, respectively. $\mathcal{O}(\cdot)$ denotes the standard big-O notation. For a vector \mathbf{x} , $\|\mathbf{x}\|$ denotes its ℓ_2 -norm, $\text{Re}\{\mathbf{x}\}$ denotes its real part, $\text{diag}(\mathbf{x})$ returns a diagonal matrix with the elements in \mathbf{x} on its main diagonal, and $[\mathbf{x}]_{a:b}$ denotes the subvector of \mathbf{x} consisting of the elements from a to b .

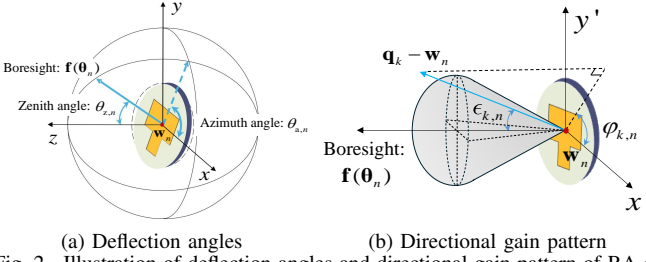


Fig. 2. Illustration of deflection angles and directional gain pattern of RA n .

For a matrix \mathbf{X} , $\text{Tr}(\mathbf{X})$ and $\text{rank}(\mathbf{X})$ denote its trace and rank, $[\mathbf{X}]_{a,b}$ denotes the (a,b) -th entry of matrix \mathbf{X} , $[\mathbf{X}]_{a:b,c:d}$ denotes the submatrix of \mathbf{X} consisting of the elements located in rows a to b and columns c to d , and $\mathbf{X} \succeq 0$ implies that \mathbf{X} is positive semi-definite. \mathbf{I} and $\mathbf{0}$ denote an identity matrix and an all-zero matrix, respectively, with appropriate dimensions. The distribution of a circularly symmetric complex Gaussian (CSCG) random vector with zero mean and covariance matrix Σ is denoted by $\mathcal{N}_c(\mathbf{0}, \Sigma)$; and \sim stands for “distributed as”.

II. SYSTEM MODEL AND PROBLEM FORMULATION

As shown in Fig. 1, we consider an RA-enabled uplink communication system, where K users (each equipped with a single isotropic antenna) simultaneously transmit their signals in the same time-frequency resource block to a BS equipped with a UPA at a fixed position consisting of N directional RAs. Without loss of generality, we assume that the UPA is placed on the x - y plane of a 3D Cartesian coordinate system and centered at the origin with $N = N_x N_y$, where N_x and N_y denote the numbers of RAs along x - and y -axes, respectively. The separation between adjacent RAs is denoted by $d \leq \frac{\lambda}{2}$, where λ denotes the signal wavelength, and the entire UPA size can be expressed as $N_x d \times N_y d$. The physical size of each RA element is denoted as $\sqrt{S} \times \sqrt{S}$ with $\sqrt{S} \leq d$, and we define $\xi \triangleq \frac{S}{d^2} \leq 1$ as the array occupation ratio of the effective antenna aperture to the overall UPA region. In general, for the hypothetical antenna element, we have $S = \frac{\lambda^2}{4\pi}$.

Assuming that both N_x and N_y are odd numbers for notational convenience, the reference position of RA n , which locates at the n_x -th column and n_y -th row on the UPA, can be expressed as

$$\mathbf{w}_n \triangleq \mathbf{w}_{n_x, n_y} \triangleq \mathbf{w}_{(n_y-1)N_x + n_x} = [n_x d, n_y d, 0]^T, \quad (1)$$

where $n_x = 0, \pm 1, \dots, \pm \frac{N_x-1}{2}$ and $n_y = 0, \pm 1, \dots, \pm \frac{N_y-1}{2}$. Let r_k denote the distance between the center of the UPA and user k , and the position of user k is then denoted by $\mathbf{q}_k = [r_k \Phi_k, r_k \Psi_k, r_k \Omega_k]^T$, with $\Phi_k \triangleq \sin \psi_k \sin \phi_k$, $\Psi_k \triangleq \cos \psi_k$, and $\Omega_k \triangleq \sin \psi_k \cos \phi_k$, where $\psi_k \in [0, \frac{\pi}{2}]$ and $\phi_k \in [0, 2\pi]$ denote the zenith and azimuth angles of user k with respect to the origin of the coordinate system, respectively. Accordingly, the distance between user k and RA n can be expressed as

$$\begin{aligned} r_{k,n} &= \|\mathbf{q}_k - \mathbf{w}_n\| \\ &= r_k \sqrt{1 - 2n_x \delta_k \Phi_k - 2n_y \delta_k \Psi_k + (n_x^2 + n_y^2) \delta_k^2}, \end{aligned} \quad (2)$$

where $\delta_k \triangleq \frac{d}{r_k}$. Note that $\delta_k \ll 1$ since the RA separation d is typically on the order of wavelength in practice.

A. Antenna Boresight Adjustment

The original orientations/boresights of all RAs are assumed to be parallel to the z -axis, and the boresight of each RA can be independently adjusted in 3D direction mechanically and/or electrically through a common smart controller. Generally speaking, mechanical control allows for a larger adjustment range in terms of antenna orientation to equivalently and coarsely change boresight direction but its response latency cannot be ignored; while electrical control can quickly and finely adjust boresight direction (without changing antenna orientation) but has a relatively limited adjustment range.

As shown in Fig. 2(a), the 3D boresight adjustment of each RA can be described by a pair of *deflection angles*: the zenith and azimuth angles with respect to the z -axis. Specifically, for RA n , the zenith angle $\theta_{z,n}$ represents the angle between the boresight direction of RA n and the z -axis, while the azimuth angle $\theta_{a,n}$ is the angle between the projection of the boresight direction of RA n onto the x - y plane and the x -axis. To characterize the 3D boresight direction of RA n , we define a pointing vector determined by the zenith angle $\theta_{z,n}$ and the azimuth angle $\theta_{a,n}$ of RA n as

$$\mathbf{f}(\boldsymbol{\theta}_n) = [\sin \theta_{z,n} \cos \theta_{a,n}, \sin \theta_{z,n} \sin \theta_{a,n}, \cos \theta_{z,n}]^T, \quad (3)$$

where $\boldsymbol{\theta}_n \triangleq [\theta_{z,n}, \theta_{a,n}]^T$ is defined as the deflection angle vector of RA n , and we have $\|\mathbf{f}(\boldsymbol{\theta}_n)\| = 1$ for normalization. To account for the antenna boresight adjustment range and to avoid antenna coupling between any two RAs, the zenith angle of each RA should be within a specific range:

$$0 \leq \theta_{z,n} \leq \theta_{\max}, \quad \forall n, \quad (4)$$

where $\theta_{\max} \in [0, \frac{\pi}{2}]$ is the maximum zenith angle that each RA is allowed to adjust.¹

B. Channel Model

The effective antenna gain for each RA depends on both the signal arrival/departure angle and antenna directional gain pattern, which characterizes the antenna radiation power distribution in different directions. In this paper, we consider a generic directional gain pattern for each RA as follows [25].

$$G_e(\epsilon, \varphi) = \begin{cases} G_0 \cos^{2p}(\epsilon), & \epsilon \in [0, \frac{\pi}{2}], \varphi \in [0, 2\pi] \\ 0, & \text{otherwise,} \end{cases} \quad (5)$$

where (ϵ, φ) is a pair of incident angles corresponding to any spatial point with respect to the RA's current boresight as shown in Fig. 2(b), p is the directivity factor that characterizes the beamwidth of the antenna's main lobe, and $G_0 = 2(2p+1)$ is the maximum gain in the boresight direction (i.e., $\epsilon = 0$) to satisfy the law of power conservation.

We consider a scattering environment with Q distributed scatterers, where the position of scatterer q is represented by $\mathbf{u}_q \in \mathbb{R}^{3 \times 1}$. Based on the *Friis Transmission Equation* and the directional gain pattern adopted in (5), and assuming the

¹To characterize the fundamental performance of the RA-enabled wireless systems, we assume that the zenith and azimuth angles of each RA can be continuously tuned in $[0, \theta_{\max}]$ and $[0, 2\pi]$, respectively, while in practice they are usually selected from a finite number of discrete values within $[0, \theta_{\max}]$ and $[0, 2\pi]$ for the ease of hardware implementation, respectively. The design of RA-enabled systems with discrete deflection angles will be left for future work.

gain of the transmit antenna at each user is normalized as $G_t = 1$, the channel power gain between user k and RA n can be modeled as [26]

$$\begin{aligned} g_{k,n}(\boldsymbol{\theta}_n) &\approx \int_{\mathbb{S}_n} \frac{1}{4\pi \|\mathbf{q}_k - \mathbf{s}\|^2} G_0 \left(\frac{\mathbf{f}^T(\boldsymbol{\theta}_n)(\mathbf{q}_k - \mathbf{s})}{\|\mathbf{q}_k - \mathbf{s}\|} \right)^{2p} d\mathbf{s} \\ &= \frac{S}{4\pi r_{k,n}^2} G_0 \cos^{2p}(\epsilon_{k,n}), \end{aligned} \quad (6)$$

where the integral space $\mathbb{S}_n = \left[n_x d - \frac{\sqrt{S}}{2}, n_x d + \frac{\sqrt{S}}{2} \right] \times \left[n_y d - \frac{\sqrt{S}}{2}, n_y d + \frac{\sqrt{S}}{2} \right]$ corresponds to the surface region of RA n , and $\cos(\epsilon_{k,n}) \triangleq \mathbf{f}^T(\boldsymbol{\theta}_n) \vec{\mathbf{q}}_{k,n} \triangleq \frac{\mathbf{q}_k - \mathbf{w}_n}{\|\mathbf{q}_k - \mathbf{w}_n\|}$ is the projection between the user k 's direction vector $\vec{\mathbf{q}}_{k,n} \triangleq \frac{\mathbf{q}_k - \mathbf{w}_n}{\|\mathbf{q}_k - \mathbf{w}_n\|}$ and the pointing vector of RA n . Similarly, the channel power gain between scatterer q and RA n is modeled as

$$m_{q,n}(\boldsymbol{\theta}_n) = \frac{S}{4\pi d_{q,n}^2} G_0 \cos^{2p}(\tilde{\epsilon}_{q,n}), \quad (7)$$

where $d_{q,n} = \|\mathbf{u}_q - \mathbf{w}_n\|$ is the distance between scatterer q and RA n , and $\cos(\tilde{\epsilon}_{q,n}) \triangleq \mathbf{f}^T(\boldsymbol{\theta}_n) \vec{\mathbf{u}}_{q,n} \triangleq \frac{\mathbf{u}_q - \mathbf{w}_n}{\|\mathbf{u}_q - \mathbf{w}_n\|}$ and the pointing vector of RA n .

For the multi-path channel between RA n and user k , by considering the geometric near-field propagation, the line-of-sight (LoS) channel component $h_{k,n}^{\text{LoS}}(\boldsymbol{\theta}_n)$ and the non-LoS (NLoS) channel component $h_{k,n}^{\text{NLoS}}(\boldsymbol{\theta}_n)$ can be separately modeled by [27], [28]

$$h_{k,n}^{\text{LoS}}(\boldsymbol{\theta}_n) = \sqrt{g_{k,n}(\boldsymbol{\theta}_n)} e^{-j\frac{2\pi}{\lambda} r_{k,n}}, \quad (8)$$

$$h_{k,n}^{\text{NLoS}}(\boldsymbol{\theta}_n) = \sum_{q=1}^Q \frac{\sqrt{\sigma_q m_{q,n}(\boldsymbol{\theta}_n)}}{t_{k,q}} e^{-j\frac{2\pi}{\lambda} (d_{q,n} + t_{k,q}) + j\chi_q}, \quad (9)$$

where σ_q represents the radar cross section (RCS) of scatterer q , modeled as an independent and identically distributed (i.i.d.) positive random variable, χ_q represents the phase shift introduced by scatterer q , and $t_{k,q} = \|\mathbf{q}_k - \mathbf{u}_q\|$ denotes the distance between user k and scatterer q . Thus, by superimposing the LoS and NLoS channel components, the overall multi-path channel between user k and the BS is given by

$$\mathbf{h}_k(\boldsymbol{\Theta}) = \mathbf{h}_k^{\text{LoS}}(\boldsymbol{\Theta}) + \mathbf{h}_k^{\text{NLoS}}(\boldsymbol{\Theta}), \quad (10)$$

where $\boldsymbol{\Theta} \triangleq [\boldsymbol{\theta}_1, \boldsymbol{\theta}_2, \dots, \boldsymbol{\theta}_N] \in \mathbb{R}^{2 \times N}$ is the deflection angle matrix of all RAs, $\mathbf{h}_k^{\text{LoS}}(\boldsymbol{\Theta}) \triangleq [h_{k,1}^{\text{LoS}}(\boldsymbol{\theta}_1), h_{k,2}^{\text{LoS}}(\boldsymbol{\theta}_2), \dots, h_{k,N}^{\text{LoS}}(\boldsymbol{\theta}_N)]^T$ and $\mathbf{h}_k^{\text{NLoS}}(\boldsymbol{\Theta}) \triangleq [h_{k,1}^{\text{NLoS}}(\boldsymbol{\theta}_1), h_{k,2}^{\text{NLoS}}(\boldsymbol{\theta}_2), \dots, h_{k,N}^{\text{NLoS}}(\boldsymbol{\theta}_N)]^T$ are the LoS and NLoS channel components between user k and the BS, respectively.

C. Min-SINR Maximization Problem

For the uplink communication, the received signal at the BS can be expressed as

$$\mathbf{y} = \sum_{k=1}^K \mathbf{h}_k(\boldsymbol{\Theta}) \sqrt{P_k} s_k + \mathbf{n}, \quad (11)$$

where P_k and s_k are the transmit power and information-bearing signal of user k , respectively, and \mathbf{n} is the additive white Gaussian noise (AWGN) vector, following the zero-mean CSCG distribution with power σ^2 , i.e., $\mathbf{n} \sim \mathcal{N}_c(\mathbf{0}, \sigma^2 \mathbf{I}_N)$. Upon receiving \mathbf{y} , the BS applies a linear

receive beamforming vector $\mathbf{v}_k^H \in \mathbb{C}^{1 \times N}$ with $\|\mathbf{v}_k\| = 1$ to extract the signal of user k , i.e.,

$$y_k = \mathbf{v}_k^H \mathbf{h}_k(\boldsymbol{\Theta}) \sqrt{P_k} s_k + \sum_{j \neq k} \mathbf{v}_k^H \mathbf{h}_j(\boldsymbol{\Theta}) \sqrt{P_j} s_j + \mathbf{v}_k^H \mathbf{n}. \quad (12)$$

Accordingly, the SINR for decoding the information from user k is given by

$$\gamma_k = \frac{\bar{P}_k |\mathbf{v}_k^H \mathbf{h}_k(\boldsymbol{\Theta})|^2}{\sum_{j \neq k} \bar{P}_j |\mathbf{v}_k^H \mathbf{h}_j(\boldsymbol{\Theta})|^2 + 1}, \quad (13)$$

where $\bar{P}_k = \frac{P_k}{\sigma^2}$ denotes user k 's equivalent transmit SNR.

In this paper, we aim to maximize the minimum SINR among all the users by jointly optimizing the receive beamforming matrix $\mathbf{V} \triangleq [\mathbf{v}_1, \mathbf{v}_2, \dots, \mathbf{v}_K]$ and deflection angle matrix $\boldsymbol{\Theta}$ of all RAs, subject to their zenith angle constraints in (4). Thus, the optimization problem is formulated as²

$$(P1): \max_{\mathbf{V}, \boldsymbol{\Theta}} \min_k \gamma_k \quad (14a)$$

$$\text{s.t. } 0 \leq \theta_{z,n} \leq \theta_{\max}, \forall n, \quad (14b)$$

$$\|\mathbf{v}_k\| = 1, \forall k. \quad (14c)$$

III. SINGLE-USER CASE WITH FREE-SPACE PROPAGATION

In this section, we consider the single-user and free-space propagation setup, i.e., $K = 1$ and $Q = 0$, to draw essential insights into (P1). Thus, the channel modeled in (10) reduces to $\mathbf{h}_1(\boldsymbol{\Theta}) = \mathbf{h}_1^{\text{LoS}}(\boldsymbol{\Theta})$. In this case, no inter-user interference is present, and thus (P1) is simplified to (by dropping the user index)

$$(P2): \max_{\mathbf{v}, \boldsymbol{\Theta}} \bar{P} |\mathbf{v}^H \mathbf{h}^{\text{LoS}}(\boldsymbol{\Theta})|^2 \quad (15a)$$

$$\text{s.t. } (14b), (14c). \quad (15b)$$

A. Optimal Closed-Form Solution

For any given RA deflection angle matrix $\boldsymbol{\Theta}$ in the single-user case, it is known that the MRC beamformer is the optimal receive beamforming solution to problem (P2) [29], i.e., $\mathbf{v}_{\text{MRC}} = \frac{\mathbf{h}^{\text{LoS}}(\boldsymbol{\Theta})}{\|\mathbf{h}^{\text{LoS}}(\boldsymbol{\Theta})\|}$. Thus, substituting \mathbf{v}_{MRC} into (15a) yields the following SNR expression,

$$\gamma = \bar{P} \|\mathbf{h}^{\text{LoS}}(\boldsymbol{\Theta})\|^2 = \frac{\bar{P} S}{4\pi} \sum_{n=1}^N \frac{G_0 \cos^{2p}(\epsilon_n)}{r_n^2}. \quad (16)$$

Exploiting the structure in (16), problem (P2) can be decomposed into N subproblems, each of which independently optimizes the deflection angle vector of one RA. For RA n , the corresponding subproblem is given by

$$(P3): \max_{\boldsymbol{\theta}_n} (\mathbf{f}^T(\boldsymbol{\theta}_n) \vec{\mathbf{q}}_n)^{2p} \quad (17a)$$

$$\text{s.t. } 0 \leq \theta_{z,n} \leq \theta_{\max}, \quad (17b)$$

where the constant term is omitted in (17a). Since $p \geq 0$, by maximizing the projection between the unit vector $\mathbf{f}(\boldsymbol{\theta}_n)$ and $\vec{\mathbf{q}}_n$, the optimal solution to problem (P3) is obtained as

$$\theta_{z,n}^* = \min \{ \arccos(\vec{\mathbf{q}}_n^T \mathbf{e}_3), \theta_{\max} \}, \quad (18a)$$

$$\theta_{a,n}^* = \arctan2(\vec{\mathbf{q}}_n^T \mathbf{e}_2, \vec{\mathbf{q}}_n^T \mathbf{e}_1), \quad (18b)$$

where $\mathbf{e}_1 = [1, 0, 0]^T$, $\mathbf{e}_2 = [0, 1, 0]^T$, and $\mathbf{e}_3 = [0, 0, 1]^T$.

²To evaluate the theoretical performance gain brought by the RA, we assume in this paper that the channel state information (CSI) of all channels involved is perfectly known at the BS. In practice, conventional channel estimation relies on correlating the received signal with a known pilot sequence transmitted from the users (e.g., least-squares (LS) estimation) can be applied at the BS to obtain the required CSI.

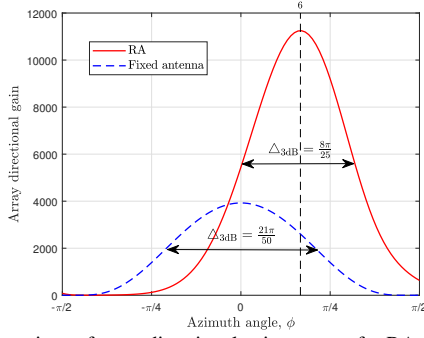


Fig. 3. Comparison of array directional gain patterns for RA and fixed-antenna arrays with $p = 4$ and $N_x = N_y = 25$.

According to the optimal RA deflection angles in (18), it can be inferred that each RA prefers to adjust its deflection angles to tune its antenna boresight towards the user. This is expected since the BS can achieve the maximum array gain NG_0 when the boresight direction of each RA is aligned with the user direction, i.e., $f(\theta_n) = \frac{\mathbf{q} - \mathbf{w}_n}{\|\mathbf{q} - \mathbf{w}_n\|}$. To demonstrate the essential changes introduced by the proposed RA architecture, based on the directional gain pattern of each antenna element given in (5), we compare the array directional gain patterns of the RA and fixed-antenna arrays in Fig. 3. For the RA array, the boresights of all RAs are adjusted to maximize the SNR in the user direction with $\psi = \frac{\pi}{2}$ and $\phi = \frac{\pi}{6}$ according to the optimal RA deflection angles in (18). It is observed that since RA array can focus its radiation power through aligning the main lobes of all antenna elements towards the desired direction, it significantly improves the array gain and narrows the beamwidth as compared to the fixed-antenna array. This result indicates that our proposed RA-enabled system has the ability to improve the communication performance by reconfiguring the array directional gain pattern according to different wireless environments and applications.

B. Asymptotic Performance Analysis

In this subsection, we focus on the performance analysis for the single-user system, including the SNR's closed-form expression, the lower/upper bounds in the ULA and UPA cases, respectively, and their corresponding asymptotic gains as the antenna number N goes to infinity. For ease of exposition, we assume that the user is located along the z -axis (i.e., $\psi = \frac{\pi}{2}$ and $\phi = 0$) and its position is denoted by $\mathbf{q} = [0, 0, r]^T$. In this case, based on the optimal zenith angle obtained in (18a), the entire array region can be divided into inner and outer areas by comparing $\arccos(\tilde{\mathbf{q}}_n^T \mathbf{e}_3)$ and θ_{\max} , as shown in Fig. 4. Specifically, if RA n is located in the inner area, we have $\arccos(\tilde{\mathbf{q}}_n^T \mathbf{e}_3) \leq \theta_{\max}$ and $\epsilon_n = 0$, i.e., RA n can adjust its boresight to perfectly align with the user direction to obtain the maximum antenna directional gain. Conversely, for RA n located in the outer area, we have $\arccos(\tilde{\mathbf{q}}_n^T \mathbf{e}_3) > \theta_{\max}$ and $\epsilon_n = \arctan(\sqrt{(n_x^2 + n_y^2)\delta^2}) - \theta_{\max}$, i.e., RA n can only serve the user with $\theta_{z,n} = \theta_{\max}$ and the RA boresight is offset from the user direction by an angle $\epsilon_n > 0$ due to the zenith angle constraint in (4). Based on the above discussion, the projection between the user direction vector and the optimal pointing vector of RA n can be expressed as

$$\cos \epsilon_n = \cos \left(\left[\arctan \left(\sqrt{(n_x^2 + n_y^2)\delta^2} \right) - \theta_{\max} \right]^+ \right), \quad (19)$$

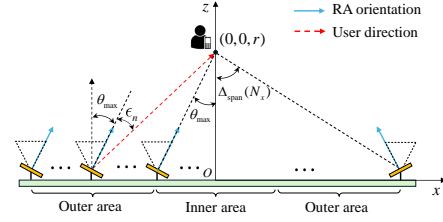


Fig. 4. Illustration of the geometric relationship between the user and RAs.

where $[x]^+ \triangleq \max\{0, x\}$. By substituting (19) into (16), we can obtain the resultant SNR as (20), shown at the top of next page. The SNR in (20) involves a double summation, which may make it difficult to gain useful insights. By approximating the double summation in (20) as its corresponding double integral by leveraging $\delta \ll 1$ as in [30]–[33], the SNR can be rewritten in an integral form as (21), also shown at the top of next page.

1) *ULA-Based RA System*: To gain some insights, we first focus on the ULA setting. With $N_y = 1$ and $N = N_x$, the resultant SNR in (21) reduces to

$$\tilde{\gamma} = \frac{\bar{P}G_0\xi\delta^2}{4\pi d} \int_{-\frac{N_x d}{2}}^{\frac{N_x d}{2}} \frac{\cos^{2p} \left(\left[\arctan \left| \frac{x}{r} \right| - \theta_{\max} \right]^+ \right)}{1 + \frac{x^2}{r^2}} dx. \quad (22)$$

It can be observed that the generic form of the SNR given by (22) is still very complicated for further analysis due to the directivity factor p of the directional gain pattern. In the following, we discuss the typical case of $p = \frac{1}{2}$, i.e., the cosine pattern based on the projected aperture.

Theorem 1: For the ULA-based RA system with cosine directional gain pattern (i.e., $p = \frac{1}{2}$) under the condition of $\delta \ll 1$, the maximum SNR achieved in the single-user setup can be expressed in closed-form as

$$\tilde{\gamma} = \begin{cases} \frac{2\bar{P}\xi\delta}{\pi} \Delta_{\text{span}}(N_x), & N_x \leq \hat{N}_x \\ \frac{2\bar{P}\xi\delta}{\pi} [\theta_{\max} + \sin(\Delta_{\text{span}}(N_x) - \theta_{\max})], & N_x > \hat{N}_x \end{cases} \quad (23)$$

where $\Delta_{\text{span}}(N_x) \triangleq \arctan \frac{N_x \delta}{2}$ denotes the *span angle* of the user, which is half of the angle formed by the two line segments connecting the user with both ends of the RA array, as illustrated in Fig. 4, and $\hat{N}_x \triangleq 2 \lfloor \frac{\tan \theta_{\max}}{\delta} \rfloor + 1$ is the maximum number of antennas in the inner area of the array.

Proof: Please refer to Appendix A. ■

Theorem 1 shows that with the applied MRC receive beamforming and the obtained optimal RA deflection angles, the resultant maximum SNR of the proposed ULA-based RA system scales with the antenna number N_x according to the span angle function $\Delta_{\text{span}}(N_x)$. Furthermore, given the antenna element size S , the antenna separation d , and the propagation distance r , the maximum SNR of the ULA-based RA system mainly depends on the allowable deflection angle range for antenna boresight adjustment and the ULA size.

Remark 1: By applying the linear approximation for the arctangent function, i.e., $\arctan(x) \approx \frac{\pi}{4}x$, $-1 \leq x \leq 1$ [35], the SNR obtained in the first case of (23) can be approximated by $\tilde{\gamma} \approx \frac{1}{2}N_x\bar{P}\xi\delta$ since we have $0 \leq \frac{N_x \delta}{2} \leq 1$ when $N_x \leq \hat{N}_x$. Thus, the resultant SNR increases linearly with the number of RAs when $N_x \leq \hat{N}_x$, i.e., $\Delta_{\text{span}}(N_x) \leq \theta_{\max}$. It can be verified that $f(x) \triangleq \sin(\arctan x - \theta_{\max})$ is a concave increasing function with respect to x and $\lim_{x \rightarrow \infty} f'(x) = 0$,

$$\gamma = \frac{\bar{P}G_0\xi\delta^2}{4\pi} \sum_{n_x=-\frac{N_x-1}{2}}^{\frac{N_x-1}{2}} \sum_{n_y=-\frac{N_y-1}{2}}^{\frac{N_y-1}{2}} \frac{\cos^{2p} \left(\left[\arctan \left(\sqrt{(n_x^2 + n_y^2)\delta^2} \right) - \theta_{\max} \right]^+ \right)}{1 + (n_x^2 + n_y^2)\delta^2}. \quad (20)$$

$$\gamma \simeq \frac{\bar{P}G_0\xi\delta^2}{4\pi d^2} \int_{-\frac{N_y d}{2}}^{\frac{N_y d}{2}} \int_{-\frac{N_x d}{2}}^{\frac{N_x d}{2}} \frac{\cos^{2p} \left(\left[\arctan \left(\sqrt{\frac{1}{r^2}(x^2 + y^2)} \right) - \theta_{\max} \right]^+ \right)}{1 + \frac{1}{r^2}(x^2 + y^2)} dx dy. \quad (21)$$

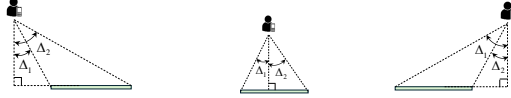


Fig. 5. Illustration of the geometric relationship between the user and ULA.

which indicates that when $N_x > \hat{N}_x$, i.e., $\Delta_{\text{span}}(N_x) > \theta_{\max}$, the growth speed of the maximum SNR slows down as the number of RAs further increases until it reaches zero.

For the infinitely large-scale ULA such that $N_x \rightarrow \infty$, since $\arctan \frac{N_x \delta}{2} \rightarrow \frac{\pi}{2}$ as $\frac{N_x \delta}{2} \rightarrow \infty$, the resultant SNR in (23) reduces to

$$\lim_{N_x \rightarrow \infty} \tilde{\gamma} = \frac{2\xi\delta}{\pi} \bar{P} (\theta_{\max} + \cos \theta_{\max}). \quad (24)$$

It is observed that a higher asymptotic SNR can be achieved for a ULA-based RA system with a larger allowable deflection angle range $[0, \theta_{\max}]$. By letting $\theta_{\max} = 0$ in (24), the asymptotic SNR for the conventional fixed-antenna system is given by³

$$\lim_{N_x \rightarrow \infty} \tilde{\gamma}_{\text{fixed}} = \frac{2\xi\delta}{\pi} \bar{P}. \quad (25)$$

Accordingly, the ratio of the asymptotic SNR of the RA system to that of the fixed-antenna system can be expressed as

$$\frac{\lim_{N_x \rightarrow \infty} \tilde{\gamma}}{\lim_{N_x \rightarrow \infty} \tilde{\gamma}_{\text{fixed}}} = \theta_{\max} + \cos \theta_{\max} \geq 1, \quad (26)$$

where the inequality holds since $f(x) = x + \cos x$ is a monotonically increasing function with respect to x and $f(0) = 1$. Therefore, by exploiting the additional spatial DoFs in terms of 3D boresights to improve the array gain, the proposed RA-enabled system with the optimal deflection angles in (18) will outperform the fixed-antenna system, and the performance gain increases with the maximum allowable zenith angle θ_{\max} .

Lemma 1: If we define the closed-form SNR given in (23) as a function with respect to the span angle of the user, i.e., $\tilde{\gamma}(\Delta_{\text{span}}(N_x))$, Theorem 1 can be extended to the general case where the user locates around the ULA with $\phi = \frac{\pi}{2}$ and an arbitrary azimuth angle $\psi \in [-\frac{\pi}{2}, \frac{\pi}{2}]$. Based on the three possible geometric relationships illustrated in Fig. 5, the resultant SNR for a given azimuth angle ψ is expressed as

$$\tilde{\gamma} = \begin{cases} \frac{1}{2\cos\psi} [\tilde{\gamma}(\Delta_2) - \tilde{\gamma}(\Delta_1)], & \text{Case 1: } \psi \in [-\frac{\pi}{2}, -\frac{N_x\delta}{2}] \\ \frac{1}{2\cos\psi} [\tilde{\gamma}(\Delta_1) + \tilde{\gamma}(\Delta_2)], & \text{Case 2: } \psi \in [-\frac{N_x\delta}{2}, \frac{N_x\delta}{2}] \\ \frac{1}{2\cos\psi} [\tilde{\gamma}(\Delta_1) - \tilde{\gamma}(\Delta_2)], & \text{Case 3: } \psi \in (\frac{N_x\delta}{2}, \frac{\pi}{2}] \end{cases} \quad (27)$$

In addition, since all geometric relationships shown in Fig. 5 will reduce to the symmetrical case in Fig. 4 when $N_x \rightarrow \infty$ regardless of ψ , the asymptotic SNR is the same as (24).

³In this paper, we assume that the boresight of each antenna is parallel to the z -axis in the fixed-antenna system for ease of exposition.

2) *UPA-Based RA System:* Next, we consider the general UPA setting to analyze its asymptotic performance. For the UPA-based RA system with a moderate physical size, assuming that the entire UPA region is within the inner area, the following lemma yields an approximate SNR.

Lemma 2: For a UPA-based RA system with $\sqrt{(N_x d)^2 + (N_y d)^2} \leq 2r \tan \theta_{\max}$ and $\theta_{\max} \leq \frac{\pi}{4}$, we have

$$\gamma \approx \frac{\bar{P}G_0\pi\xi\delta^2}{64} N_x N_y. \quad (28)$$

Proof: Please refer to Appendix B. ■

Lemma 2 shows that when the entire UPA region is located in the inner area, the SNR with MRC beamforming and optimal RA deflection angles increases linearly with the antenna number $N = N_x N_y$.

For a large RA array where the UPA region exceeds the inner area, it is challenging to obtain a closed-form expression for (21) due to the double integral and the circular boundary between the inner and outer areas. Alternatively, we first derive its lower/upper bounds for drawing useful insights as follows.

Theorem 2: For the UPA-based RA system, defining $R_{\text{lb}} = \frac{1}{2}\min\{N_x d, N_y d\}$ and $R_{\text{ub}} = \frac{1}{2}\sqrt{(N_x d)^2 + (N_y d)^2}$ as the radii of the inscribed and circumscribed disks of the rectangular region $N_x d \times N_y d$ occupied by the UPA, the resultant SNR is lower-/upper-bounded by

$$\mathcal{G}(R_{\text{lb}}, p, \theta_{\max}) \leq \gamma \leq \mathcal{G}(R_{\text{ub}}, p, \theta_{\max}), \quad (29)$$

where the function $\mathcal{G}(R, p, \theta_{\max})$ is defined as

$$\mathcal{G}(R, p, \theta_{\max}) = \frac{\bar{P}G_0\xi}{2} \left[\frac{1}{2} \ln \left(1 + \left(\frac{D}{r} \right)^2 \right) + \int_{\arctan \frac{D}{r} - \theta_{\max}}^{\arctan \frac{R}{r} - \theta_{\max}} \cos^{2p} \epsilon \tan(\epsilon + \theta_{\max}) d\epsilon \right], \quad (30)$$

with $D \triangleq \min\{R, r \tan \theta_{\max}\}$ being the radius of the inner area in which the RAs can adjust their boresights to align with the user direction.

Proof: Please refer to Appendix C. ■

In (30), the first integral corresponds to the inner area with $\epsilon_n = 0$, while the second integral corresponds to the outer area with $\epsilon_n > 0$. The integral in (30) is challenging to handle since the directivity factor p exists as a power exponent of the cosine function. Similar to the ULA case, we focus on the cosine gain pattern (i.e., $p = \frac{1}{2}$) for convenience in the following discussion.

Lemma 3: For $p = \frac{1}{2}$, the function $\mathcal{G}(R, p, \theta_{\max})$ can be expressed in closed form as (31), shown at the top of the next page, where $\theta_R \triangleq \arctan \frac{R}{r}$.

Proof: Please refer to Appendix D. ■

By combining Theorem 2 and Lemma 3, the lower/upper bounds for an RA-enabled system can be obtained according

$$\mathcal{G}\left(R, \frac{1}{2}, \theta_{\max}\right) = \begin{cases} \bar{P}\xi \ln(1 + \tan^2 \theta_R), \\ 2\bar{P}\xi \left[1 - \ln(\cos \theta_{\max}) - \cos(\theta_R - \theta_{\max}) + \sin \theta_{\max} \ln\left(\frac{(1+\sin \theta_R)(1-\sin \theta_{\max})}{\cos \theta_R \cos \theta_{\max}}\right)\right], \end{cases} \begin{array}{l} R \leq r \tan \theta_{\max} \\ R > r \tan \theta_{\max}. \end{array} \quad (31)$$

to the UPA size. To obtain the lower/upper bounds for the fixed-antenna system, we set $\theta_{\max} = 0$ in (30) and calculate the integral in a manner similar to Appendix D, yielding

$$\mathcal{G}\left(R, \frac{1}{2}, 0\right) = 2\bar{P}\xi (1 - \cos \theta_R). \quad (32)$$

For the case of $\theta_{\max} > 0$, the inequality $\mathcal{G}(R, \frac{1}{2}, \theta_{\max}) > 2\bar{P}\xi \left[1 - \cos \theta_R + \sin \theta_{\max} \left(\ln \frac{1+\sin \theta_R}{\cos \theta_R} + \ln \frac{1-\sin \theta_{\max}}{1-\sin^2 \theta_{\max}}\right)\right] > \mathcal{G}(R, \frac{1}{2}, 0)$ must hold, indicating that the SNR's lower bound of the RA system is always higher than that of the fixed-antenna system when $R_{lb} > r \tan \theta_{\max}$. As the UPA size $N_x d, N_y d \rightarrow \infty$, the radii of the inscribed and circumscribed disks of the UPA region $N_x d \times N_y d$ go to infinity, i.e., $R_{lb}, R_{ub} \rightarrow \infty$. Therefore, the lower/upper bounds given by Theorem 2 approach to the same limit due to the identical form of the function $\mathcal{G}(R, p, \theta_{\max})$ as $R \rightarrow \infty$. Based on the above, we draw a conclusion that for the UPA setting, the RA system also achieves a higher asymptotic SNR than the fixed-antenna system, like the previous ULA case.

IV. MULTI-USER CASE UNDER MULTI-PATH CHANNEL

In this section, we consider the general multi-user and multi-path channel setup, i.e., $K > 1$ and $Q \geq 0$. Specifically, an AO algorithm and a two-stage algorithm are proposed to solve problem (P1) suboptimally, which offer different tradeoffs between system performance and computational complexity.

A. AO Algorithm

To overcome the challenges posed by the non-concavity of the objective function in (14a) and the intricate coupling between the receive beamforming vectors $\{\mathbf{v}_k\}$ and the RA deflection angle vectors $\{\boldsymbol{\theta}_n\}$, an AO algorithm is proposed to alternately optimize the receive beamforming and RA deflection angles in an iterative manner for the multi-user system.

1) *Receive Beamforming Optimization*: For given RA deflection angle matrix $\boldsymbol{\Theta}$, the channel from user k to the BS modeled in (10) becomes fixed. Accordingly, problem (P1) reduces to (by simplifying $\mathbf{h}_k(\boldsymbol{\Theta})$ to \mathbf{h}_k)

$$(P4): \max_{\mathbf{V}} \min_k \frac{\bar{P}_k |\mathbf{v}_k^H \mathbf{h}_k|^2}{\sum_{j \neq k} \bar{P}_j |\mathbf{v}_k^H \mathbf{h}_j|^2 + 1} \quad (33a)$$

$$\text{s.t. (14c).} \quad (33b)$$

The SINR in (13) is a generalized Rayleigh quotient with respect to \mathbf{v}_k , and the receive SINR for each user can be maximized by the MMSE beamforming [37], [38]. Thus, the optimal solution to problem (P4) can be obtained as

$$\mathbf{v}_k^{\text{MMSE}} = \frac{\mathbf{C}_k^{-1} \mathbf{h}_k}{\|\mathbf{C}_k^{-1} \mathbf{h}_k\|}, \quad \forall k, \quad (34)$$

where $\mathbf{C}_k \triangleq \sum_{j \neq k} \bar{P}_j \mathbf{h}_j \mathbf{h}_j^H + \mathbf{I}_N$ is the interference-plus-noise covariance matrix. To reduce the dimension of matrix inversion from $N \times N$ to $(K-1) \times (K-1)$, by applying the *Woodbury matrix identity*, \mathbf{C}_k^{-1} is equivalently expressed as

$$\begin{aligned} \mathbf{C}_k^{-1} &= (\mathbf{I}_N + \bar{\mathbf{H}}_k \mathbf{P}_k \bar{\mathbf{H}}_k^H)^{-1} \\ &= \mathbf{I}_N - \bar{\mathbf{H}}_k (\mathbf{P}_k^{-1} + \bar{\mathbf{H}}_k^H \bar{\mathbf{H}}_k)^{-1} \bar{\mathbf{H}}_k^H. \end{aligned} \quad (35)$$

2) *RA Deflection Angle Optimization*: For given receive beamforming matrix \mathbf{V} , by introducing the slack optimization variable η to denote the minimum SINR, problem (P1) can be written as

$$(P5): \max_{\eta, \boldsymbol{\Theta}} \eta \quad (36a)$$

$$\text{s.t. } \gamma_k \geq \eta, \quad \forall k, \quad (36b)$$

$$(14b). \quad (36c)$$

The above subproblem is still challenging to solve since constraint (36b) is non-convex and the deflection angles, i.e., $\theta_{z,n}$ and $\theta_{a,n}$, are coupled in the pointing vector $\mathbf{f}(\boldsymbol{\theta}_n)$.

Note that the pointing vector $\mathbf{f}(\boldsymbol{\theta}_n)$ is essentially a unit vector on the unit sphere, and the RA deflection angles mainly affect the channel power gains through the projections $\cos(\epsilon_{k,n})$ and $\cos(\tilde{\epsilon}_{k,n})$ as shown in (6) and (7). For ease of subsequent derivation, we introduce an auxiliary variable $\mathbf{f}_n \in \mathbb{R}^{3 \times 1}$ with $\|\mathbf{f}_n\| = 1$ to equivalently replace the influence of deflection angle vector $\boldsymbol{\theta}_n$ on the pointing vector of RA n , i.e., $\mathbf{f}_n \triangleq \mathbf{f}(\boldsymbol{\theta}_n)$. Thus, based on (8) and (9), the multi-path channel between user k and RA n can be rewritten as

$$\tilde{h}_{k,n}(\mathbf{f}_n) = \alpha_{k,n} (\mathbf{f}_n^T \vec{\mathbf{q}}_{k,n})^p + \sum_{q=1}^Q \beta_{k,n,q} (\mathbf{f}_n^T \vec{\mathbf{u}}_{q,n})^p, \quad (37)$$

where $\alpha_{k,n} \triangleq \frac{1}{r_{k,n}} \sqrt{\frac{SG_0}{4\pi}} e^{-j \frac{2\pi}{\lambda} r_{k,n}}$ and $\beta_{k,n,q} \triangleq \frac{1}{d_{q,n} t_{k,q}} \sqrt{\frac{SG_0 \sigma_q}{4\pi}} e^{-j \frac{2\pi}{\lambda} (d_{q,n} + t_{k,q}) + j\chi_q}$. Let $\mathbf{F} \triangleq [\mathbf{f}_1, \mathbf{f}_2, \dots, \mathbf{f}_N]$ and $\tilde{\mathbf{h}}_k(\mathbf{F}) \triangleq [\tilde{h}_{k,1}(\mathbf{f}_1), \tilde{h}_{k,2}(\mathbf{f}_2), \dots, \tilde{h}_{k,N}(\mathbf{f}_N)]^T$, and problem (P7) can be transformed into

$$(P6): \max_{\eta, \mathbf{F}} \eta \quad (38a)$$

$$\text{s.t. } \frac{\bar{P}_k |\mathbf{v}_k^H \tilde{\mathbf{h}}_k(\mathbf{F})|^2}{\sum_{j \neq k} \bar{P}_j |\mathbf{v}_k^H \tilde{\mathbf{h}}_j(\mathbf{F})|^2 + 1} \geq \eta, \quad \forall k, \quad (38b)$$

$$\mathbf{f}_n^T \mathbf{e}_3 \geq \cos(\theta_{\max}), \quad \forall n, \quad (38c)$$

$$\|\mathbf{f}_n\| = 1, \quad \forall n, \quad (38d)$$

where constraint (38c) is equivalent to (14b) and constraint (38d) ensures that \mathbf{f}_n is a unit vector.

To deal with the fractional structure on the left hand side of constraint (38b), we take the logarithmic operation on both sides of constraint (38b), resulting in an equivalent form for constraint (38b), i.e.,

$$\ln(\bar{P}_k |\mathbf{v}_k^H \tilde{\mathbf{h}}_k(\mathbf{F})|^2) \geq \ln(\eta) + \ln\left(\sum_{j \neq k} \bar{P}_j |\mathbf{v}_k^H \tilde{\mathbf{h}}_j(\mathbf{F})|^2 + 1\right), \quad (39)$$

which is still difficult to handle since $\tilde{h}_{k,n}(\mathbf{f}_n)$ in (37) is neither convex nor concave due to the complex coefficients $\alpha_{k,n}$ and $\{\beta_{k,n,q}\}$. To tackle this challenge, we adopt the SCA technique to approximate constraint (39) as a convex constraint and obtain a local optimal solution to problem (P6) in an iterative manner. Without loss of generality, we present the procedure of the $(i+1)$ -th iteration and denote the solutions of \mathbf{F} and η obtained in the i -th iteration by $\mathbf{F}^{(i)}$ and $\eta^{(i)}$, respectively. By using the first-order Taylor expansion at $\{\mathbf{f}_n^{(i)}\}$, $|\mathbf{v}_k^H \tilde{\mathbf{h}}_k(\mathbf{F})|^2$

$$\Lambda_k^{(i+1)}(\mathbf{F}) \triangleq |\mathbf{v}_k^H \tilde{\mathbf{h}}_k(\mathbf{F}^{(i)})|^2 + \operatorname{Re} \left\{ \left(\mathbf{v}_k^H \tilde{\mathbf{h}}_k(\mathbf{F}^{(i)}) \right)^* \sum_{n=1}^N v_{k,n}^* \tilde{h}'_{k,n} (\mathbf{f}_n - \mathbf{f}_n^{(i)}) \right\}. \quad (40)$$

$$\Gamma_k^{(i+1)}(\mathbf{F}) \triangleq \ln \left(\sum_{j=1, j \neq k}^K \bar{P}_j |\mathbf{v}_k^H \tilde{\mathbf{h}}_j(\mathbf{F}^{(i)})|^2 + 1 \right) + \frac{\sum_{j=1, j \neq k}^K \bar{P}_j \operatorname{Re} \left\{ \left(\mathbf{v}_k^H \tilde{\mathbf{h}}_j(\mathbf{F}^{(i)}) \right)^* \sum_{n=1}^N v_{k,n}^* \tilde{h}'_{j,n} (\mathbf{f}_n - \mathbf{f}_n^{(i)}) \right\}}{\sum_{j=1, j \neq k}^K \bar{P}_j |\mathbf{v}_k^H \tilde{\mathbf{h}}_j(\mathbf{F}^{(i)})|^2 + 1}. \quad (41)$$

and $\ln \left(\sum_{j=1, j \neq k}^K \bar{P}_j |\mathbf{v}_k^H \tilde{\mathbf{h}}_j(\mathbf{F})|^2 + 1 \right)$ in (39) can be respectively linearized as $\Lambda_k^{(i+1)}(\mathbf{F})$ and $\Gamma_k^{(i+1)}(\mathbf{F})$, shown at the top of the next page, where $\tilde{h}'_{k,n} \triangleq \frac{\partial h_{k,n}(\mathbf{f}_n^{(i)})}{\partial \mathbf{f}_n^{(i)}} = \tilde{\alpha}_{k,n} \vec{\mathbf{q}}_{k,n}^T + \sum_{q=1}^Q \tilde{\beta}_{k,n,q} \vec{\mathbf{u}}_{q,n}^T$ with $\tilde{\alpha}_{k,n} \triangleq \alpha_{k,n} p ((\mathbf{f}_n^{(i)})^T \vec{\mathbf{q}}_{k,n})^{p-1}$ and $\tilde{\beta}_{k,n,q} \triangleq \beta_{k,n,q} p ((\mathbf{f}_n^{(i)})^T \vec{\mathbf{u}}_{q,n})^{p-1}$. Similarly, an upper bound for $\ln(\eta)$ is obtained as $\Xi^{(i+1)}(\eta) \triangleq \ln(\eta^{(i)}) + \frac{\eta}{\eta^{(i)}} - 1$ by using its first-order Taylor expansions at $\eta^{(i)}$. In this way, constraint (39) can be approximated by

$$\ln \left(\bar{P}_k \Lambda_k^{(i+1)}(\mathbf{F}) \right) \geq \Gamma_k^{(i+1)}(\mathbf{F}) + \Xi^{(i+1)}(\eta), \quad \forall k. \quad (42)$$

Thus, problem (P6) can be approximated by the following problem in the $(i+1)$ -th iteration.

$$(P7): \max_{\eta, \mathbf{F}} \eta \quad (43a)$$

$$\text{s.t. (38c), (38d), (42).} \quad (43b)$$

Problem (P7) is still non-convex due to the unit constraint for \mathbf{f}_n . For convenience, we first relax the equality constraint (38d) as $\|\mathbf{f}_n\| \leq 1$, yielding the following problem.

$$(P8): \max_{\eta, \mathbf{F}} \eta \quad (44a)$$

$$\text{s.t. } \|\mathbf{f}_n\| \leq 1, \forall n, \quad (44b)$$

$$(38c), (42). \quad (44c)$$

It can be verified that problem (P8) is a convex optimization problem, which can be solved by the CVX solver [36]. Note that the optimal value obtained by problem (P8) serves as an upper bound for that of problem (P7) due to the relaxation of the equality constraint (38d).

3) *Overall Algorithm*: We summarize the proposed AO algorithm in Algorithm 1. Since the optimal objective value η is non-decreasing over iterations and must be upper-bounded, Algorithm 1 is guaranteed to converge. The complexity order of Algorithm 1 is $\mathcal{O}(L(KN^3 + N^{3.5} \ln(1/\varepsilon)))$, where L denotes the required iteration number for algorithm convergence.

After obtaining the optimal solutions of \mathbf{V} and \mathbf{F} through Algorithm 1, the pointing vector needs to be recovered as a unit vector, i.e., $\mathbf{f}_n^* = \frac{\mathbf{f}_n}{\|\mathbf{f}_n\|}$. Furthermore, the original problem aims to obtain the RA deflection angle matrix Θ , and thus an additional step is needed to transform the optimized pointing vector into the desired deflection angles. For RA n , based on the obtained pointing vector \mathbf{f}_n^* , the corresponding RA deflection angle vector θ_n^* can be obtained as

$$\theta_{z,n}^* = \arccos((\mathbf{f}_n^*)^T \mathbf{e}_3), \quad (45a)$$

$$\theta_{a,n}^* = \arctan2((\mathbf{f}_n^*)^T \mathbf{e}_2, (\mathbf{f}_n^*)^T \mathbf{e}_1). \quad (45b)$$

As a result, the optimal minimum SINR η^* can be calculated by substituting the obtained \mathbf{V}^* and Θ^* into (13).

B. Two-Stage Algorithm

In this subsection, we propose another low-complexity algorithm, namely the two-stage algorithm, to solve problem

Algorithm 1 Proposed AO Algorithm for Solving (P1).

- 1: Input: Pointing vector $\mathbf{F}^{(0)}$, minimum receive SINR $\eta^{(0)}$, and threshold $\varepsilon > 0$.
- 2: Initialization: $i \leftarrow 0$.
- 3: **repeat**
- 4: Given $\mathbf{F}^{(i)}$, calculate $\mathbf{V}^{(i+1)}$ according to (34).
- 5: Given $\mathbf{V}^{(i+1)}$, $\mathbf{F}^{(i)}$, and $\eta^{(i)}$, obtain $\mathbf{F}^{(i+1)}$ and $\eta^{(i+1)}$ by solving problem (P8).
- 6: Update $i = i + 1$.
- 7: **until** $|\frac{\eta^{(i+1)} - \eta^{(i)}}{\eta^{(i)}}| \leq \varepsilon$.
- 8: Output: $\mathbf{V} = \mathbf{V}^{(i)}$ and $\mathbf{F} = \mathbf{F}^{(i)}$.

(P1) without the need for iteration. Specifically, the deflection angles of all RAs are optimized based on the semidefinite relaxation (SDR) technique in the first stage, and the corresponding beamforming vector is obtained by ZF beamformer in the second stage.

As observed in Section IV-A, the difficulty in optimizing the pointing vectors mainly comes from the exponent with power p in the antenna's directional gain pattern as shown in (5) and the fractional structure of the SINR. According to the law of power conservation, as the directivity factor p increases, the maximum antenna gain G_0 in the boresight direction becomes larger and the antenna main lobe becomes narrower. Nevertheless, the variation in parameter p does not change the relative magnitude relationship of radiation power in different directions. As such, we consider a typical value of p to eliminate the exponent structure. Specifically, for the cosine-square gain pattern with $p = 1$, the multi-path channel between user k and RA n modeled in (37) is expressed as the following linear combination form,

$$\hat{h}_{k,n} = \mathbf{f}_n^T \mathbf{a}_{k,n}, \quad (46)$$

where $\mathbf{a}_{k,n} \triangleq \alpha_{k,n} \vec{\mathbf{q}}_{k,n} + \sum_{q=1}^Q \beta_{k,n,q} \vec{\mathbf{u}}_{q,n}$.

The ZF receive beamforming is adopted to completely remove the inter-user interference, which requires $N \geq K$. Thus, by applying the ZF receive beamforming, the SINR reduces to an SNR without inter-user interference. For user k , the ZF receive beamforming, denoted by \mathbf{v}_k^{ZF} , should satisfy $(\mathbf{v}_k^{\text{ZF}})^H \bar{\mathbf{H}}_k = \mathbf{0}_{1 \times (K-1)}$ with $\bar{\mathbf{H}}_k \triangleq [\mathbf{h}_1, \dots, \mathbf{h}_{k-1}, \mathbf{h}_{k+1}, \dots, \mathbf{h}_K]$. Therefore, the ZF receive beamforming for user k is expressed as

$$\mathbf{v}_k^{\text{ZF}} = \frac{(\mathbf{I}_N - \bar{\mathbf{H}}_k (\bar{\mathbf{H}}_k^H \bar{\mathbf{H}}_k)^{-1} \bar{\mathbf{H}}_k^H) \mathbf{h}_k}{\|(\mathbf{I}_N - \bar{\mathbf{H}}_k (\bar{\mathbf{H}}_k^H \bar{\mathbf{H}}_k)^{-1} \bar{\mathbf{H}}_k^H) \mathbf{h}_k\|}, \quad \forall k, \quad (47)$$

where $\mathbf{I}_N - \bar{\mathbf{H}}_k (\bar{\mathbf{H}}_k^H \bar{\mathbf{H}}_k)^{-1} \bar{\mathbf{H}}_k^H$ is the projection matrix into the space orthogonal to the columns of $\bar{\mathbf{H}}_k$. By substituting (47) into (13), the resultant SINR for user k with ZF beamforming is given by

$$\gamma_{\text{ZF},k} = \bar{P}_k \|\mathbf{h}_k\|^2 (1 - \rho_{\text{ZF},k}), \quad (48)$$

where $\rho_{\text{ZF},k} = \frac{\mathbf{h}_k^H \bar{\mathbf{H}}_k (\bar{\mathbf{H}}_k^H \bar{\mathbf{H}}_k)^{-1} \bar{\mathbf{H}}_k^H \mathbf{h}_k}{\|\mathbf{h}_k\|^2}$ with $0 \leq \rho_{\text{ZF},k} \leq 1$ denoting the SNR loss factor caused by the cancellation of inter-user interference with ZF beamforming. According to (48), the resultant SINR for user k based on ZF beamforming mainly depends on channel power gain $\|\mathbf{h}_k\|^2$ when the SNR loss factor $\rho_{\text{ZF},k}$ is given by a reasonable value.

1) *First stage:* Let $\hat{\mathbf{a}}_k \triangleq [\mathbf{a}_{k,1}^T, \mathbf{a}_{k,2}^T, \dots, \mathbf{a}_{k,N}^T]^T \in \mathbb{C}^{3N \times 1}$ and $\hat{\mathbf{f}} \triangleq [\mathbf{f}_1^T, \mathbf{f}_2^T, \dots, \mathbf{f}_N^T]^T \in \mathbb{R}^{3N \times 1}$. Then, we formulate the following problem to optimize the pointing vectors.

$$(\text{P9}): \max_{\hat{\mathbf{f}}, \omega} \omega \quad (49\text{a})$$

$$\text{s.t. } \rho_k \bar{P}_k \|\hat{\mathbf{f}}^T \hat{\mathbf{a}}_k\|^2 \geq \omega, \forall k, \quad (49\text{b})$$

$$\hat{\mathbf{f}}_{3(n-1)+1:3n}^T \mathbf{e}_1 \geq \cos \theta_{\max}, \forall n, \quad (49\text{c})$$

$$\|\hat{\mathbf{f}}_{3(n-1)+1:3n}\|^2 = 1, \forall n, \quad (49\text{d})$$

where ρ_k can be initially set as $\rho_k = 1 - \rho_{\text{ZF},k}$ based on (48) with $\Theta = \mathbf{0}$, serving as a weight factor for user k to be balanced for maximizing the channel power gains of all users, and constraints (49c) and (49d) are equivalent to (38c) and (38d), respectively. Note that $\|\hat{\mathbf{f}}^T \hat{\mathbf{a}}_k\|^2 = \hat{\mathbf{f}}^T \mathbf{A}_k \hat{\mathbf{f}} = \text{Tr}(\mathbf{A}_k \hat{\mathbf{f}} \hat{\mathbf{f}}^T)$ with $\mathbf{A}_k = \hat{\mathbf{a}}_k \hat{\mathbf{a}}_k^H$. Define $\hat{\mathbf{F}} = \hat{\mathbf{f}} \hat{\mathbf{f}}^T$, which needs to satisfy $\hat{\mathbf{F}} \succeq \mathbf{0}$ and $\text{rank}(\hat{\mathbf{F}}) = 1$. Since the rank-one constraint is non-convex, we apply semidefinite relaxation (SDR) technique to relax this constraint. As a result, problem (P9) is transformed into

$$(\text{P10}): \max_{\hat{\mathbf{F}}, \omega} \omega \quad (50\text{a})$$

$$\text{s.t. } \rho_k \bar{P}_k \text{Tr}(\mathbf{A}_k \hat{\mathbf{F}}) \geq \omega, \forall k, \quad (50\text{b})$$

$$\hat{\mathbf{F}}_{3(n-1)+1:3(n-1)+1} \geq \cos^2 \theta_{\max}, \forall n, \quad (50\text{c})$$

$$\text{Tr}(\hat{\mathbf{F}}_{3(n-1)+1:3n, 3(n-1)+1:3n}) = 1, \forall n, \quad (50\text{d})$$

$$\hat{\mathbf{F}} \succeq \mathbf{0}. \quad (50\text{e})$$

As problem (P10) is a convex semidefinite program (SDP), it can be optimally solved by the CVX solver with a complexity order of $\mathcal{O}((3N)^{3.5})$ [39], and we represent the optimal solution to $\hat{\mathbf{F}}$ by $\hat{\mathbf{F}}^*$.

Since problem (P10) may not lead to a rank-one solution of $\hat{\mathbf{F}}$, the optimal objective value of problem (P10) serves as an upper bound of problem (P9). Thus, a rank-one approximation on $\hat{\mathbf{F}}^*$ should be executed as an additional step to construct a feasible solution to problem (P9). If $\hat{\mathbf{F}}^*$ is rank-one, we have $\hat{\mathbf{F}}^* = \hat{\mathbf{f}}^* \hat{\mathbf{f}}^{*T}$, and $\hat{\mathbf{f}}^*$ will be a feasible and optimal solution to problem (P9). On the other hand, if the rank of $\hat{\mathbf{F}}^*$ is larger than one, we define $\tilde{\mathbf{f}} = \sqrt{\lambda_{\max}} \mathbf{m}_{\max}$ with λ_{\max} and \mathbf{m}_{\max} denoting the maximum eigenvalue and its corresponding eigenvector obtained through eigenvalue decomposition of $\hat{\mathbf{F}}^*$, respectively, as our candidate solution to problem (P9) since the best rank-one approximation to $\hat{\mathbf{F}}^*$ is given by $\hat{\mathbf{F}}^* = \lambda_{\max} \mathbf{m}_{\max} \mathbf{m}_{\max}^T$ [39].

2) *Second Stage:* After obtaining the stacked pointing vector $\hat{\mathbf{f}}^*$ in the first stage and letting $\mathbf{f}_n = \hat{\mathbf{f}}_{3(n-1)+1:3n}^*, \forall n$, we reconstruct the RA deflection angles similar to (45) and the channel conditions according to (8)–(10). Then, the corresponding ZF beamforming can be readily calculated by (47).

Remark 2: Although the two-stage algorithm may experience some performance loss by limiting $p = 1$, it has lower complexity without the need for iteration. In contrast, the AO algorithm, while having higher computational complexity, is

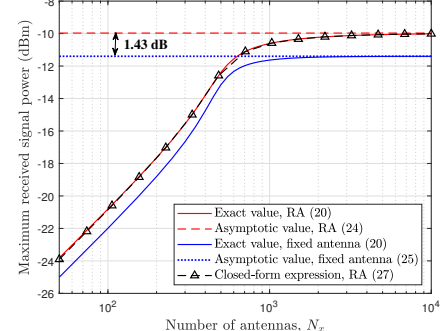


Fig. 6. Maximum received signal power versus the number of antennas N_x for the ULA-based single-user system.

applicable to any value of p . It is worth noting that both the AO and two-stage algorithms can also be applied to the single-user setup with arbitrary Q scatterers by replacing the MMSE/ZF receive beamforming of (34)/(47) with MRC beamforming. Nevertheless, for the single-user setup with $Q = 0$, since the AO and two-stage algorithms can only achieve suboptimal solutions and result in higher computational complexity, they are much less efficient than the optimal closed-form solution derived in (18) of Section III-A.

V. SIMULATION RESULTS

In this section, we present simulation results to evaluate the performance of our proposed RA-enabled communication system as well as the optimization algorithms for the joint design of receive beamforming and RA deflection angles. In the following simulations, we assume the system operates at 2.4 GHz with a wavelength of $\lambda = 0.125$ meter (m), the noise power at the BS is set to $\sigma^2 = -80$ dBm, the antenna separation is $d = \frac{\lambda}{2}$, and the size of each antenna is $S = \frac{\lambda^2}{8\pi}$.

The RCS of scatterer q is modeled as $\sigma_q = \frac{4\pi s_q^2}{\lambda^2}$, where s_q denotes the effective echo surface area of scatterer q and it is randomly generated within $[0, 1]$, and the introduced phase shift χ_q is generated through an i.i.d. random variable with uniform distribution over $[-\pi, \pi]$. Unless otherwise stated, the transmit power of all users is set to the same value, i.e., $P_k = P = 20$ dBm, $\forall k$, and the maximum zenith angle allowed for RA boresight adjustment is $\theta_{\max} = \frac{\pi}{6}$.

A. Single-User System

First, we consider a single-user system under free-space propagation, where the distance between the center of the array and the user is set to $r = 15$ m. In this subsection, we consider only the cosine gain pattern (i.e., $p = \frac{1}{2}$) to validate the performance analysis in Section III-B. The received signal power P_R at the BS, which is proportional to the resultant SNR due to the relationship $P_R = \sigma^2 \gamma$, is considered as the performance metric.

To compare the directional gains of RA and fixed-antenna systems, Fig. 6 plots the maximum received signal power versus the number of antennas N_x for a ULA-based system. The received signal power is obtained by averaging over various user directions. The asymptotic values given in (24) and (25) are also shown in the figure. It is first observed that the closed-form SNR derived in (27) matches perfectly with the exact value calculated by (20), which validates the correctness of

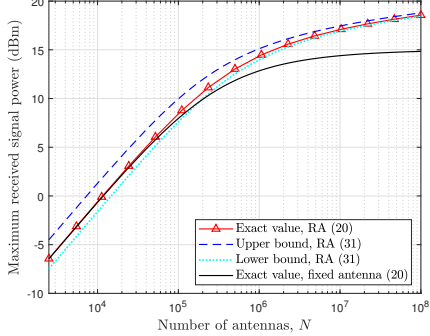


Fig. 7. Maximum received signal power versus the number of antennas N for the square UPA-based single-user system.

Theorem 1 and Lemma 1. Additionally, for a small to moderate number of antennas, the received signal powers of both the RA and fixed-antenna systems increase linearly with N_x , which is in accordance with Remark 1. However, as N_x further increases, it is observed that due to the limited deflection angle range for antenna boresight adjustment, the received signal powers of both RA and fixed-antenna systems increase slowly and eventually approach to their asymptotic values. Furthermore, due to the additional spatial DoFs induced by the antenna boresight adjustment for improving the array directional gain, RA system reaches its asymptotic limit later and achieves up to 1.43 dB gain over the fixed-antenna system, which corroborates the accuracy of analytical result in (26) as $10\log_{10} \lim_{N_x \rightarrow \infty} \tilde{\gamma} = 10\log_{10} \left(\frac{\pi}{6} + \cos \frac{\pi}{6} \right) \approx 1.43$ dB. Based on this result, we can also infer that with a larger antenna directivity factor p , the RA system will exhibit a more pronounced array gain over the fixed-antenna system due to the higher directional gain in the boresight direction of each antenna towards the user.

In Fig. 7, we plot the received signal power versus the number of antennas for a square UPA-based system, where $N_x = N_y$ and the position of the user is given by $[0, 0, r]^T$. First, it can be observed that for the RA system, both the analytical lower and upper bounds in (31) are quite tight and accurate to the exact value of the received signal power calculated via (20). With a small to moderate number of antennas, the received signal powers of both the RA and fixed-antenna systems increase linearly with N , which is in accordance with our approximation in Lemma 2. As the number of antennas further increases, the performance advantage of the RA system over the fixed-antenna system becomes more significant. This is because the beam direction will deviate from the boresight direction of the antenna located at the edge of the array in the fixed-antenna system, which degrades the array gain. Instead, this deviation can be effectively circumvented by adjusting the antenna boresight direction to align with the user direction as closely as possible.

Fig. 8 shows the received signal power versus the azimuth angle of the user for a square UPA, where the zenith angle of the user is given by $\psi = \frac{\pi}{2}$. As ϕ increases from 0 to $\frac{\pi}{3}$ or decreases from 0 to $-\frac{\pi}{3}$, the received signal power of the fixed-antenna system drastically decreases. This is due to the fact that the array directional gain pattern of the fixed-antenna system is fixed and the radiation power only focuses

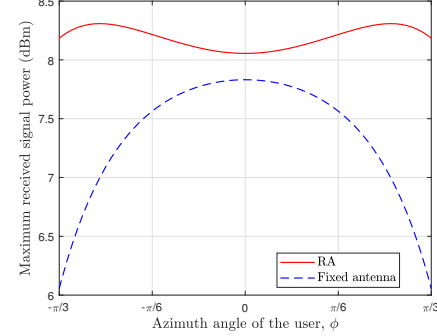


Fig. 8. Maximum received signal power versus the azimuth angle of the user ϕ for the UPA-based single-user system with $N_x = N_y = 201$.

on the region directly in front of the array as shown in Fig. 3. In contrast, the gain pattern of the RA array can be flexibly reconfigured to improve the directional gain in the user direction, even when the user directly faces one of the two ends of the array. It can be observed that the RA array helps the BS achieve more stable and uniform received signal power over the entire angular region as compared to the fixed-antenna system. The above results indicate that RA array has the potential to uniformly enhance communication coverage performance in its front half-space.

B. Multi-User System

Next, we consider a multi-user system under the multi-path channel model with $K = 4$ users and $Q = 3$ scatterers, and their geometric relationships are shown in Fig. 9. Specifically, four users lie evenly on a half circle centered at the BS array with a radius of $d_1 = 50$ m, and three scatterers are randomly located within three disk regions with a radius of $d_3 = 2$ m, which lie evenly on a half circle centered at the center of the BS array with a radius of $d_2 = 25$ m. A square UPA-based system with $N_x = N_y = 9$ is considered. In the following, we present simulation results by averaging over 100 independent channel realizations, and the max-min achievable rate (which monotonically increases with the SINR) among all the K users is considered as the performance metric, which is given by

$$C = \min_k \log_2 (1 + \gamma_k) = \log_2 \left(1 + \min_k \gamma_k \right). \quad (51)$$

To validate the performance advantages of our proposed RA-enabled system, we consider the following three benchmark schemes for comparison:

- **Random orientation design:** In this scheme, the deflection angles of each RA, i.e., $\{\theta_{z,n}\}$ and $\{\theta_{a,n}\}$, are randomly generated following a uniform distribution within $[0, \theta_{\max}]$ and $[0, 2\pi]$, respectively, and the MMSE receive beamforming is applied at the BS.
- **Array-wise orientation adjustment:** In this scheme, we adjust the orientation of the entire antenna array instead of that of each antenna element. To achieve the max-min achievable rate, by applying the MMSE receive beamforming, the optimal zenith and azimuth angles of the antenna array are obtained by using exhaustive search within $[0, \theta_{\max}]$ and $[0, 2\pi]$, respectively.
- **Without orientation adjustment (i.e., fixed-antenna system):** In this scheme, the orientations of all RAs are

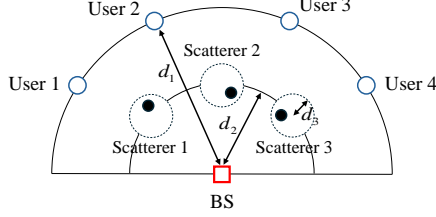


Fig. 9. Simulation setup of the multi-user and multi-path channel case.

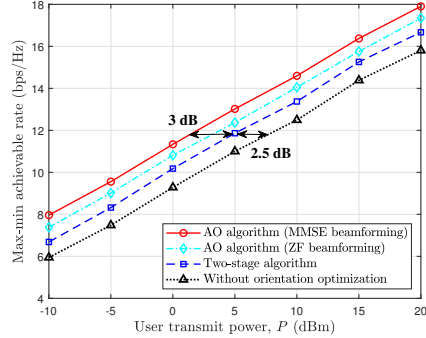


Fig. 10. Max-min achievable rates obtained by different optimization algorithms versus the user transmit power P .

fixed as their reference orientations, i.e., $\Theta = \mathbf{0}$, and the MMSE receive beamforming is applied at the BS.

In Fig. 10, we compare the max-min achievable rates versus the user transmit power P for different optimization algorithms. First, it is observed that the AO algorithm with MMSE receive beamforming obtains the highest max-min achievable rate and achieves up to 3 dB gain over the two-stage algorithm. As discussed in Remark 2, this gain gap is expected since the lack of iteration and the assumption of $p = 1$ in the two-stage algorithm will inevitably cause performance loss. Second, by optimizing the deflection angles of all RAs to maximize the minimum weighted channel power gain with much lower computational complexity than the AO algorithm, the two-stage algorithm still achieves up to 2.5 dB gain over the fixed-antenna system without orientation/boresight optimization. The above results indicate the different tradeoffs between performance and complexity offered by the two proposed algorithms. Furthermore, since the ZF receiver enhances the noise power, the AO algorithm with MMSE beamforming always outperforms that with ZF beamforming.

Fig. 11 shows the max-min achievable rates of different schemes versus the maximum zenith angle θ_{\max} . Several interesting observations are made as follows. First, as the maximum zenith angle θ_{\max} increases, the proposed RA system gains more DoFs and flexibilities to balance the array directional gain over the multi-path channels, thus leading to a further increase in its max-min achievable rate. Second, the proposed RA system always outperforms both the array-wise orientation adjustment counterpart and the fixed-antenna system. This is because neither of the latter two systems can independently adjust the orientation of each antenna to reconfigure the directional gain pattern of the entire array, and the radiation power is distributed only directly in front of the array. Third, since the RAs with random orientations can statistically radiate power in any direction of the BS to

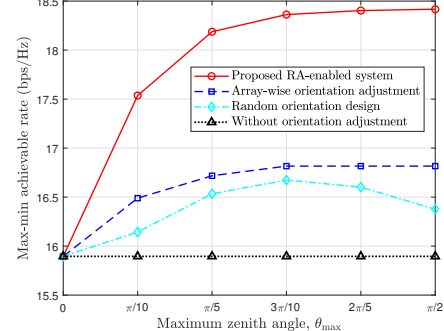


Fig. 11. Max-min achievable rates of different schemes versus the maximum zenith angle θ_{\max} .

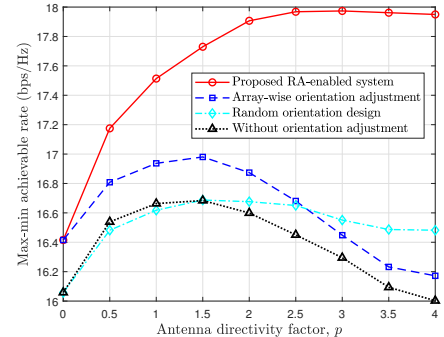


Fig. 12. Max-min achievable rates of different systems versus the antenna directivity factor p .

serve spatially-distributed users, it can achieve a higher max-min achievable rate than the fixed-antenna system. However, when $\theta_{\max} \geq \frac{3\pi}{10}$, the max-min achievable rate of the random orientation design scheme slightly declines with θ_{\max} . This result highlights the importance of antenna orientation/boresight optimization in an RA system, since the random orientations will lead to an unordered array directional gain pattern and inevitable performance loss when θ_{\max} is large enough. Last but not least, it is interesting to note that the growth speed of the max-min achievable rate obtained by our proposed RA-enabled system substantially increases when $\theta_{\max} \leq \frac{\pi}{10}$, which indicates that even with a small deflection angle range for RA orientation/boresight adjustment, the proposed RA-enabled system with optimized deflection angles can achieve significant performance improvement.

Fig. 12 shows the max-min achievable rates of different schemes versus the antenna directivity factor p . It is observed that the max-min achievable rate of the proposed RA-enabled system increases with the directivity factor p . This can be explained by the fact that with a larger p , the directional gain in the boresight direction of the antenna becomes larger and the main lobe becomes narrower, which is more advantageous for our RA-enabled system to enhance directional gains in multiple user directions by adjusting the orientations/boresights of RAs, thus resulting in a larger max-min achievable rate. In contrast, the max-min achievable rates of the array-wise orientation adjustment scheme and the fixed-antenna system decrease with p when $p \geq 1.5$. The reason for this is that with a larger directivity factor p , the radiation power of both schemes will be more concentrated in the region directly in front of the array. As a result, the directional gains for users deviating

from the main direction of the array will become weaker, thus resulting in a lower max-min achievable rate. Additionally, although the random orientation design scheme can disperse the radiation power of the array in multiple specific directions, it is significantly inferior to the proposed RA-enabled system since it fails to strategically allocate the antenna resources to fairly improve the communication performance of all users. The above results highlight the necessity of our proposed RA-enabled system for increasing channel capacity, especially in situations where the antennas have strong directivity, i.e., the main lobes are narrow.

VI. CONCLUSION

In this paper, we proposed a new RA model that provides new spatial DoFs to reconfigure the array directional gain pattern by flexibly adjusting the 3D orientation/boresight of each antenna, thus substantially enhancing the array gain and transmission rate without increasing the number of antennas or changing antenna positions. Specifically, the receive beamforming and the deflection angles of all RAs were jointly optimized to maximize the minimum SINR among all users. The optimal closed-form RA deflection angles were first derived with MRC receive beamforming applied in the single-user and free-space propagation setup. Meanwhile, the asymptotic performance analysis for the case with an infinitely large number of antennas showed that the RA-enabled system always achieves a higher array gain as compared to the conventional fixed-antenna system. For the general multi-user and multi-path channel setup, an AO algorithm and a two-stage algorithm were proposed to obtain high-quality suboptimal solutions to balance the array directional gain over the multi-path channels. Simulation results validated our analytical results and demonstrated that our proposed RA-enabled system significantly outperforms various benchmark schemes. It was shown that even with a small deflection angle range for RA boresight adjustment, the RA-enabled system could still reap considerable performance gains.

APPENDIX A

PROOF OF THEOREM 1

First, for the case of $p = \frac{1}{2}$ and $N_x \leq \hat{N}_x \triangleq 2 \left\lfloor \frac{\tan \theta_{\max}}{\delta} \right\rfloor + 1$, the integral in (22) can be simplified as

$$\begin{aligned} \mathbb{D} &= \int_{-\frac{N_x \delta}{2}}^{\frac{N_x \delta}{2}} \frac{1}{1 + \frac{x^2}{r^2}} dx = 2r \int_0^{\frac{N_x \delta}{2}} \frac{1}{1 + x^2} dx \\ &= 2r \arctan x \Big|_0^{\frac{N_x \delta}{2}} = 2r \arctan \frac{\hat{N}_x \delta}{2}. \end{aligned} \quad (52)$$

Then, for $N_x > \hat{N}_x$, the integral in (22) can be calculated as

$$\begin{aligned} \mathbb{D} &= 2 \left[\int_0^{\frac{\hat{N}_x \delta}{2}} \frac{1}{1 + \frac{x^2}{r^2}} dx + \int_{\frac{\hat{N}_x \delta}{2}}^{\frac{N_x \delta}{2}} \frac{\cos(\arctan \frac{x}{r} - \theta_{\max})}{1 + \frac{x^2}{r^2}} dx \right] \\ &\stackrel{(a)}{=} 2r \left[\int_0^{\frac{\hat{N}_x \delta}{2}} \frac{1}{1 + x^2} dx + \int_{\frac{\hat{N}_x \delta}{2}}^{\frac{N_x \delta}{2}} \frac{\cos \theta_{\max} + \sin \theta_{\max} x}{(1 + x^2)^{\frac{3}{2}}} dx \right] \\ &\stackrel{(b)}{=} 2r \left[\arctan x \Big|_0^{\frac{\hat{N}_x \delta}{2}} + \frac{\cos \theta_{\max} x - \sin \theta_{\max}}{\sqrt{1 + x^2}} \Big|_{\frac{\hat{N}_x \delta}{2}}^{\frac{N_x \delta}{2}} \right] \\ &\stackrel{(c)}{=} 2r \left[\theta_{\max} + \sin \left(\arctan \frac{N_x \delta}{2} - \theta_{\max} \right) \right], \end{aligned} \quad (53)$$

where (a) holds due to $\cos(\arctan(x)) = \frac{1}{\sqrt{1+x^2}}$ and $\sin(\arctan(x)) = \frac{x}{\sqrt{1+x^2}}$, (b) follows the integral formulas 2.103.4, 2.264.5 and 2.264.6 in [34], and (c) holds due to the fact that $\arctan \frac{\hat{N}_x \delta}{2} = \theta_{\max}$.

Thus, based on (52) and (53), the proof of Theorem 1 is completed.

APPENDIX B PROOF OF LEMMA 2

For the case of $\sqrt{(N_x d)^2 + (N_y d)^2} \leq 2r \tan \theta_{\max}$, i.e., $\epsilon_n = 0, \forall n$, the SNR expression in (21) reduces to

$$\gamma = \frac{\bar{P} G_0 \xi \delta^2}{4\pi d^2} \int_{-\frac{N_y \delta}{2}}^{\frac{N_y \delta}{2}} \int_{-\frac{N_x \delta}{2}}^{\frac{N_x \delta}{2}} \frac{1}{1 + \frac{1}{r^2}(x^2 + y^2)} dx dy. \quad (54)$$

By first integrating x and then y , the double integral in (54) can be calculated as

$$\begin{aligned} \mathbb{D} &= r^2 \int_{-\frac{N_y \delta}{2}}^{\frac{N_y \delta}{2}} \int_{-\frac{N_x \delta}{2}}^{\frac{N_x \delta}{2}} \frac{1}{1 + x^2 + y^2} dx dy \\ &\stackrel{(d)}{=} r^2 \int_{-\frac{N_y \delta}{2}}^{\frac{N_y \delta}{2}} \frac{1}{\sqrt{1 + y^2}} \arctan \frac{x}{\sqrt{1 + y^2}} dy \Big|_{-\frac{N_x \delta}{2}}^{\frac{N_x \delta}{2}} \\ &= r^2 \int_{-\frac{N_y \delta}{2}}^{\frac{N_y \delta}{2}} \frac{2}{\sqrt{1 + y^2}} \arctan \frac{N_x \delta}{2\sqrt{1 + y^2}} dy \\ &\stackrel{(e)}{\approx} \frac{1}{4} N_x \pi \delta r^2 \int_{-\frac{N_y \delta}{2}}^{\frac{N_y \delta}{2}} \frac{1}{1 + y^2} dy \\ &= \frac{1}{4} N_x \pi \delta r^2 \arctan y \Big|_{-\frac{N_y \delta}{2}}^{\frac{N_y \delta}{2}} \\ &= \frac{1}{2} N_x \pi \delta r^2 \arctan \frac{N_y \delta}{2} \\ &\stackrel{(f)}{\approx} \frac{N_x N_y \pi^2 \delta^2 r^2}{16}, \end{aligned} \quad (55)$$

where (d) follows the integral formula 2.172 in [34], (e) and (f) hold by exploiting the linear approximation of $\arctan(x) \approx \frac{\pi}{4}x, -1 \leq x \leq 1$ [35].

Thus, by substituting (55) into (54) and considering the conditions that $-1 \leq \frac{N_x \delta}{2} \leq 1$ and $-1 \leq \frac{N_y \delta}{2} \leq 1$, i.e., $N_x, N_y \leq \frac{2}{\delta}$ or $\theta_{\max} \leq \frac{\pi}{4}$, Lemma 2 can be obtained.

APPENDIX C PROOF OF THEOREM 2

Based on Theorem 1 in [33] and the approximated SNR expression in (21), we have

$$\mathcal{F}(R_{lb}, p, \theta_{\max}) \leq \gamma \leq \mathcal{F}(R_{ub}, p, \theta_{\max}), \quad (56)$$

where the function $\mathcal{F}(R, p, \theta_{\max})$ is defined as

$$\begin{aligned} \mathcal{F}(R, p, \theta_{\max}) &= \frac{\bar{P} G_0 \xi \delta^2}{4\pi d^2} \left(\int_0^{2\pi} d\zeta \int_0^D \frac{1}{1 + \left(\frac{l}{r}\right)^2} l dl + \right. \\ &\quad \left. \int_0^{2\pi} d\zeta \int_D^R \frac{\cos^{2p} \left(\arctan \frac{l}{r} - \theta_{\max} \right)}{1 + \left(\frac{l}{r}\right)^2} l dl \right), \end{aligned} \quad (57)$$

where $D \triangleq \min\{R, r \tan \theta_{\max}\}$. The first double integral in (57) can be calculated as

$$\begin{aligned} \mathbb{D}_1 &= 2\pi r^2 \int_0^{\frac{D}{r}} \frac{ldl}{1+l^2} = \pi r^2 \ln(1+l^2) \Big|_0^{\frac{D}{r}} \\ &= \pi r^2 \ln \left(1 + \left(\frac{D}{r} \right)^2 \right). \end{aligned} \quad (58)$$

The second double integral in (57) can be calculated as

$$\begin{aligned} \mathbb{D}_2 &= 2\pi r^2 \int_{\frac{D}{r}}^{\frac{R}{r}} \frac{\cos^{2p}(\arctan l - \theta_{\max})}{1+l^2} ldl \\ &= 2\pi r^2 \int_{\arctan \frac{D}{r} - \theta_{\max}}^{\arctan \frac{R}{r} - \theta_{\max}} \cos^{2p} \epsilon \tan(\epsilon + \theta_{\max}) d\epsilon. \end{aligned} \quad (59)$$

Thus, by substituting (58) and (59) into (56) and (57), Theorem 1 can be obtained.

APPENDIX D PROOF OF LEMMA 3

For $p = \frac{1}{2}$, the integral in (30) can be calculated as

$$\begin{aligned} \mathbb{D} &= \int_{\arctan \frac{D}{r}}^{\arctan \frac{R}{r}} \cos(\epsilon - \theta_{\max}) \tan \epsilon d\epsilon \\ &= \int_{\arctan \frac{D}{r}}^{\arctan \frac{R}{r}} \left(\cos \theta_{\max} \sin \epsilon + \sin \theta_{\max} \frac{\sin^2 \epsilon}{\cos \epsilon} \right) d\epsilon \\ &= \cos \theta_{\max} \left(\cos \left(\arctan \frac{D}{r} \right) - \cos \left(\arctan \frac{R}{r} \right) \right) + \\ &\quad \sin \theta_{\max} \int_{\sin(\arctan \frac{D}{r})}^{\sin(\arctan \frac{R}{r})} \frac{\epsilon^2}{1-\epsilon^2} d\epsilon \\ &\stackrel{(g)}{=} \cos \theta_{\max} (\cos \theta_{\max} - \cos \theta_R) + \\ &\quad \sin \theta_{\max} \left(\frac{1}{2} \ln \left(\frac{1+\epsilon}{1-\epsilon} \right) - \epsilon \right) \Big|_{\sin \theta_{\max}}^{\sin \theta_R} \\ &= 1 - \cos(\theta_R - \theta_{\max}) + \\ &\quad \frac{\sin \theta_{\max}}{2} \ln \left(\frac{(1+\sin \theta_R)(1-\sin \theta_{\max})}{(1-\sin \theta_R)(1+\sin \theta_{\max})} \right), \end{aligned} \quad (60)$$

where $\theta_R \triangleq \arctan \frac{R}{r}$, (g) follows the integral formulas 2.147.1 and 2.111.6 in [34], and it has $\theta_{\max} = \arctan \frac{D}{r}$ when $R \geq D$.

Thus, by substituting (60) into (30), Lemma 3 can be obtained.

REFERENCES

- [1] C.-X. Wang *et al.*, "On the road to 6G: Visions, requirements, key technologies, and testbeds," *IEEE Commun. Surveys Tuts.*, vol. 25, no. 2, pp. 905–974, 2nd Quart., 2023.
- [2] T. E. Bogale and L. B. Le, "Massive MIMO and mmWave for 5G wireless HetNet: Potential benefits and challenges," *IEEE Veh. Technol. Mag.*, vol. 11, no. 1, pp. 64–75, Feb. 2016.
- [3] L. Lu, G. Y. Li, A. L. Swindlehurst, A. Ashikhmin, and R. Zhang, "An overview of massive MIMO: Benefits and challenges," *IEEE J. Sel. Topics Signal Process.*, vol. 8, no. 5, pp. 742–758, Oct. 2014.
- [4] B. Zheng, C. You, W. Mei, and R. Zhang, "A survey on channel estimation and practical passive beamforming design for intelligent reflecting surface aided wireless communications," *IEEE Commun. Surveys Tuts.*, vol. 24, no. 2, pp. 1035–1071, 2nd Quart., 2022.
- [5] Y. Liu *et al.*, "Near-field communications: A tutorial review," *IEEE Open J. Commun. Soc.*, vol. 4, pp. 1999–2049, Aug. 2023.
- [6] H. Lu *et al.*, "A tutorial on near-field XL-MIMO communications towards 6G," *IEEE Commun. Surveys Tuts.*, vol. 26, no. 4, pp. 2213–2257, 4th Quart., 2024.
- [7] W. K. New *et al.*, "A tutorial on fluid antenna system for 6G networks: Encompassing communication theory, optimization methods and hardware designs," *IEEE Commun. Surveys Tuts.*, Early Access, 2024.
- [8] K.-K. Wong, A. Shojaeifard, K.-F. Tong, and Y. Zhang, "Fluid antenna systems," *IEEE Trans. Wireless Commun.*, vol. 20, no. 3, pp. 1950–1962, Mar. 2021.
- [9] L. Zhu, W. Ma, and R. Zhang, "Movable antennas for wireless communication: Opportunities and challenges," *IEEE Commun. Mag.*, vol. 62, no. 6, pp. 114–120, Jun. 2024.
- [10] L. Zhu, W. Ma, and R. Zhang, "Modeling and performance analysis for movable antenna enabled wireless communications," *IEEE Trans. Wireless Commun.*, vol. 23, no. 6, pp. 6234–6250, Jun. 2024.
- [11] W. Ma, L. Zhu, and R. Zhang, "MIMO capacity characterization for movable antenna systems," *IEEE Trans. Wireless Commun.*, vol. 23, no. 4, pp. 3392–3407, Apr. 2024.
- [12] K.-K. Wong and K.-F. Tong, "Fluid antenna multiple access," *IEEE Trans. Wireless Commun.*, vol. 21, no. 7, pp. 4801–4815, Jul. 2022.
- [13] W. K. New, K.-K. Wong, H. Xu, K.-F. Tong, and C.-B. Chae, "An information-theoretic characterization of MIMO-FAS: Optimization, diversity-multiplexing tradeoff and q-outage capacity," *IEEE Trans. Wireless Commun.*, vol. 23, no. 6, pp. 5541–5556, Jun. 2024.
- [14] L. Zhu, W. Ma, and R. Zhang, "Movable-antenna array enhanced beamforming: Achieving full array gain with null steering," *IEEE Commun. Lett.*, vol. 27, no. 12, pp. 3340–3344, Dec. 2023.
- [15] H. Qin, W. Chen, Q. Wu, Z. Zhang, Z. Li, and N. Cheng, "Cramér-rao bound minimization for movable antenna-assisted multiuser integrated sensing and communications," *IEEE Wireless Commun. Lett.*, vol. 13, no. 12, pp. 3404–3408, Dec. 2024.
- [16] W. Liu, X. Zhang, H. Xing, J. Ren, Y. Shen, and S. Cui, "UAV-enabled wireless networks with movable-antenna array: Flexible beamforming and trajectory design," *IEEE Wireless Commun. Lett.*, Early Access, 2024.
- [17] F. Rostami Ghadi, K.-K. Wong, W. K. New, H. Xu, R. Murch, and Y. Zhang, "On performance of RIS-aided fluid antenna systems," *IEEE Wireless Commun. Lett.*, vol. 13, no. 8, pp. 2175–2179, Aug. 2024.
- [18] X. Wei, W. Mei, Q. Wu, B. Ning, and Z. Chen, "Movable antennas meet intelligent reflecting surface: When do we need movable antennas?" *arXiv preprint arXiv: 2408.15668*, Sep. 2024.
- [19] B. Zheng, X. Xiong, T. Ma, D. W. K. Ng, A. L. Swindlehurst, and R. Zhang, "Intelligent reflecting surface-enabled anti-detection for secure sensing and communications," *IEEE Wireless Commun.*, Early Access, 2024.
- [20] D. Zhang, S. Ye, M. Xiao, K. Wang, M. D. Renzo, and M. Skoglund, "Fluid antenna array enhanced over-the-air computation," *IEEE Wireless Commun. Lett.*, vol. 13, no. 6, pp. 1541–1545, Jun. 2024.
- [21] X. Shao, Q. Jiang, and R. Zhang, "6D movable antenna based on user distribution: Modeling and optimization," *IEEE Trans. Wireless Commun.*, Early Access, 2024.
- [22] X. Shao, R. Zhang, Q. Jiang, and R. Schober, "6D movable antenna enhanced wireless network via discrete position and rotation optimization," *IEEE J. Sel. Areas Commun.*, Early Access, 2024.
- [23] X. Shao and R. Zhang, "6DMA enhanced wireless network with flexible antenna position and rotation: Opportunities and challenges," *IEEE Commun. Mag.*, Early Access, 2024.
- [24] X. Shao, R. Zhang, and R. Schober, "Exploiting six-dimensional movable antenna for wireless sensing," *IEEE Wireless Commun. Lett.*, 2024, Early Access, 2024.
- [25] C. A. Balanis, *Antenna theory: Analysis and Design*. John Wiley & Sons, 2015.
- [26] H. T. Friis, "A note on a simple transmission formula," *Proceedings of the IRE*, vol. 34, no. 5, pp. 254–256, May. 1946.
- [27] Y. Lu and L. Dai, "Near-field channel estimation in mixed LoS/NLoS environments for extremely large-scale MIMO systems," *IEEE Trans. Commun.*, vol. 71, no. 6, pp. 3694–3707, Jun. 2023.
- [28] Z. Dong and Y. Zeng, "Near-field spatial correlation for extremely large-scale array communications," *IEEE Commun. Lett.*, vol. 26, no. 7, pp. 1534–1538, Jul. 2022.
- [29] D. Tse and P. Viswanath, *Fundamentals of Wireless Communication*. Cambridge, U.K.: Cambridge Univ. Press, 2005.
- [30] H. Lu and Y. Zeng, "How does performance scale with antenna number for extremely large-scale MIMO?" in *Proc. IEEE Int. Conf. Commun. (ICC)*, Jun. 2021, pp. 1–6.
- [31] H. Lu and Y. Zeng, "Communicating with extremely large-scale array/surface: Unified modeling and performance analysis," *IEEE Trans. Wireless Commun.*, vol. 21, no. 6, pp. 4039–4053, Jun. 2022.

- [32] B. Zheng and R. Zhang, "Simultaneous transmit diversity and passive beamforming with large-scale intelligent reflecting surface," *IEEE Trans. Wireless Commun.*, vol. 22, no. 2, pp. 920–933, Feb. 2023.
- [33] C. Feng, H. Lu, Y. Zeng, T. Li, S. Jin, and R. Zhang, "Near-field modeling and performance analysis for extremely large-scale IRS communications," *IEEE Trans. Wireless Commun.*, vol. 23, no. 5, pp. 4976–4989, May 2024.
- [34] I. S. Gradshteyn and I. M. Ryzhik, *Table of Integrals, Series, and Products*, 7th ed. Cambridge, MA, USA: Academic, 2007.
- [35] S. Rajan, S. Wang, R. Inkol, and A. Joyal, "Efficient approximations for the arctangent function," *IEEE Signal Process. Mag.*, vol. 23, no. 3, pp. 108–111, May 2006.
- [36] S. Boyd and L. Vandenberghe, *Convex Optimization*. Cambridge, U.K.: Cambridge Univ. Press, Mar. 2004.
- [37] B. Zheng, C. You and R. Zhang, "Double-IRS assisted multi-user MIMO: Cooperative passive beamforming design," *IEEE Trans. Wireless Commun.*, vol. 20, no. 7, pp. 4513–4526, Jul. 2021.
- [38] H. Lu and Y. Zeng, "Near-field modeling and performance analysis for multi-user extremely large-scale MIMO communication," *IEEE Commun. Lett.*, vol. 26, no. 2, pp. 277–281, Feb. 2022.
- [39] Z.-Q. Luo, W.-K. Ma, A. So, Y. Ye, and S. Zhang, "Semidefinite relaxation of quadratic optimization problems," *IEEE Signal Process. Mag.*, vol. 27, no. 3, pp. 20–34, May 2010.